Chapter 2
Theoretical Background

This chapter introduces the fundamental physics and concepts of dielectrics [1–10] and their classification [9–17], as well as of ferroelectrics [8–25], and relaxor ferroelectrics [26–32]. The information of many textbooks and review papers related to the physics of materials science was employed throughout these sections. Unless explicitly stated otherwise, mathematical relationships displayed throughout this work hold for linear and homogeneous materials. For more detailed mathematical treatments the reader is referred to Refs. [11, 12].

2.1 Dielectrics

Dielectrics are electrically insulating materials. Gauss's law indicates that the free charge density ρ_{fr} of a dielectric medium enclosed by a surface leads to an electric displacement D_i,[1] as given in Eq. 2.1.

$$\nabla_i \cdot D_i = \rho_{fr}, \tag{2.1}$$

where ∇_i is the nabla operator. It is convenient to define the concept of an order parameter. An order parameter is a scalar or tensor variable of state that is defined such that its thermal or compositional average is distinguishable in the different phases or states of a system. For instance, D_i can be considered as an order parameter in the case of a dielectric medium where two different phases or states develop with different thermal or compositional averages of this quantity.

Upon the application of an external electric field E_i, a dielectric medium will react by forming a density of permanent and/or induced electric dipole moments. This leads to the formation of a macroscopic polarization density P_i, as expressed in Eq. 2.2.

[1]Subscripts indicate tensor variables. In case no tensor notation is used, the variable is either a scalar or the norm of the variable considered. The Einstein convention of repeated indexes is used for all tensor relations.

M. Acosta, *Strain Mechanisms in Lead-Free Ferroelectrics for Actuators*,
Springer Theses, DOI 10.1007/978-3-319-27756-1_2

$$P_i = D_i - \varepsilon_0 E_i, \tag{2.2}$$

where ε_0 is the permittivity of vacuum, given by $\varepsilon_0 = \frac{1}{\mu_0 C^2} = 8.854118 \times 10^{-12}$ F/m (μ_0: vacuum permeability, C: speed of light). The term $\varepsilon_0 E_i$ describes the vacuum contribution caused by the application of the external electric field E_i. According to Eq. 2.1, the presence of free charges, generates a D_i that can be calculated using Eq. 2.3 in the presence of E_j.

$$D_i = \varepsilon_{ij} E_j = \varepsilon_0 \varepsilon_r^{ij} E_j, \tag{2.3}$$

where ε_{ij} is the permittivity of the medium, ε_r^{ij}[2] is the relative permittivity and is a dimensionless physical quantity defined as the ratio between ε_{ij} and ε_0.

All order parameters can be modified by a thermodynamic external conjugate variable. Note that for simplicity, only the relevant relationships to this work will be introduced. In the case of D_i, its conjugate variable is E_j. From Eqs. 2.2 and 2.3 a proportionality between P_i and E_j can be deduced (Eq. 2.4), and thus P_i can also be defined as an order parameter with E_j being its conjugate.

$$P_i = \varepsilon_0 \varepsilon_r^{ij} E_j - \varepsilon_0 E_j = \varepsilon_0 E_j \left(\varepsilon_r^{ij} - 1\right) = \varepsilon_0 \chi_{ij} E_j, \tag{2.4}$$

where $\chi_{ij} = \varepsilon_r^{ij} - 1$ is the dielectric susceptibility. In the case of dielectrics where $\varepsilon_r^{ij} \gg 1$, $P_i \approx \varepsilon_0 \varepsilon_r^{ij} E_j \approx D_i$.

Equations 2.2–2.4 describe the mean linear properties of a dielectric medium. The order parameter P_i in dielectrics is coupled to other order parameters such as strain gradient $\frac{\partial S_{ij}}{\partial x_j}$ (where S_{ij} is the strain tensor and x_j position). Additionally, P_i is coupled to $\emptyset_i$, which represents either octahedral tilting for perovskites or rotation angle around a helical or spiral axis for structures with handedness [33]. Only perovskite dielectrics are relevant to this work, so $\emptyset_i$ will only be considered as the octahedral tilt angle. Coupling between P_i and $\frac{\partial S_{ij}}{\partial x_j}$ is termed flexoelectricity, while the coupling between P_i and $\emptyset_i$ is designated as rotoelectricity. Equation 2.5 introduces the influence of the aforementioned couplings to P_i for the case of a material subjected to E_j, $\frac{\partial S_{jk}}{\partial x_l}$, and $\emptyset_j$.

$$P_i = \varepsilon_0 \chi_{ij} E_j + \mu_{ijkl} \frac{\partial S_{jk}}{\partial x_l} + r_{ijk} \emptyset_j \emptyset_k, \tag{2.5}$$

where μ_{ijkl} is the flexoelectric coefficient and r_{ijk} is the rotoelectricity coefficient. A converse relationship can be constructed relating strain S_{ij} to other order parameters. This establishes several strain mechanisms for dielectrics displayed in Eq. 2.6.

[2]For proper reading, indexes of tensor variables with subscripts are displayed as upper scripts.

$$S_{ij} = Q_{ijkl} P_k P_l - \mu_{ijkl} \frac{\partial P_k}{\partial x_l} + R_{ijkl} \emptyset_k \emptyset_l, \tag{2.6}$$

where Q_{ijkl} is the electrostrictive coefficient and the non-linear term that comprises it is known as the electrostrictive effect. The R_{ijkl} is termed the rotostriction coefficient and is the converse effect of rotoelectricity. The converse effect of flexoelectricity is represented by the second term of Eq. 2.6. Note that electrostriction does not possess a direct effect (i.e., it is not present in Eq. 2.5). This is due to the fact that the order parameter S_{ij} obtained by its conjugate thermodynamic variable stress σ_{ij} will not break the center of symmetry as it acts on mass points. However, E_i acts on charge points and thus breaks the center of symmetry of a dielectric leading to non-zero S_{ij}. Rotoelectricity, electrostriction, and rotostriction are higher-order terms that are proportional to even orders of their respective conjugate thermodynamic variables. Thus a change in polarity of their conjugate thermodynamic variable does not modify the resulting P_i or S_{ij}. Odd terms of P_i coupled to $\emptyset_i$ are not introduced in Eq. 2.6 since they are rarely encountered in nature. The presence of odd electrostrictive terms indicates piezoelectricity. Odd electrostrictive terms are forbidden in several dielectrics depending on their symmetry, as will be discussed in Sect. 2.2.

The macroscopic approach introduced so far neglects the microscopic origin of P_i. Alternatively to the constitutive equations of state described, P_i can also be obtained by adding all the k dipole moments p^i of a dielectric material, as depicted in Eq. 2.7.

$$P_i = \sum_k N_k p_k^i. \tag{2.7}$$

The microscopic origin of p^i in materials is due to five different mechanisms:

- *Electronic polarization* exists in all dielectrics and is based on the displacement of the negatively charged electron shell against the positively charged atomic nucleus.
- *Ionic polarization* exists in ionic materials due to the displacement of positive and negative sublattices under electric field.
- *Orientational polarization* is a result of the alignment of permanent dipoles in a material under an electric field.
- *Space charge polarization* exists in dielectrics that feature spatial heterogeneities of charge carrier densities and is commonly found in materials with grain boundaries with different electrical conductivity than the bulk. This contribution is also denominated Maxwell-Wagner polarization.
- *Domain wall polarization* is relevant only for ferroelectrics. It is a result of the movement of the boundaries that separate differently oriented polarization volumes, as it will be treated in Sect. 2.2.1.

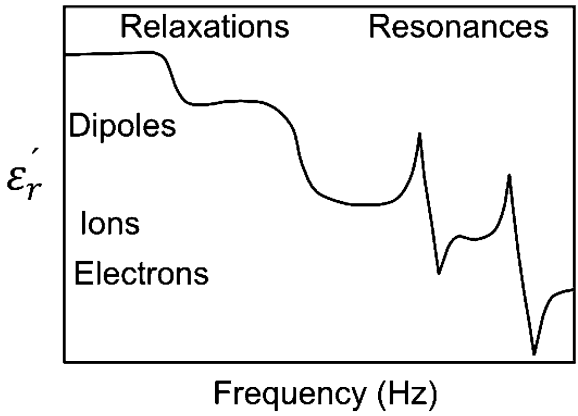

Fig. 2.1 Frequency dependence of real part of the relative permittivity ε_r'

Electronic and ionic polarization mechanisms are lattice contributions and thus termed intrinsic. Orientational polarization, space charge, and domain wall polarization are not a result of the lattice itself and thus are termed extrinsic contributions. Each polarization contribution is characterized by a distinctive microscopic polarizability α_i giving rise to a local electric field E^i_{local}. Therefore, Eq. 2.7 can be alternatively expressed as displayed in Eq. 2.8.

$$P_i = \sum_k N_k \alpha_k^i E^i_{local}(k). \tag{2.8}$$

These microscopic polarization responses can be distinguished by characteristic response frequencies, as displayed in Fig. 2.1.

The characteristic time response of each microscopic polarization mechanism under alternating electric field leads to dielectric losses and thus complex variables are required to represent the ε_r^{ij}. Since Eqs. 2.7 and 2.8 relate microscopic and macroscopic variables, macroscopic variables may also depict complex values. In an ideal, loss-free dielectric there is a phase difference between current and voltage of 90° indicating that ε_r^{ij} is a real-valued tensor. However, in dielectrics with finite conductivity, ε_r^{ij} is a complex-valued tensor such as displayed in Fig. 2.2. The phase angle $\theta = 90^0 - \delta$ determines the phase difference between the real part (ε_r') and the imaginary part (ε_r''). Therefore, the tangent of the angle δ (i.e., tan δ) is normally designated as the loss factor of dielectrics.

2.2 Classification of Dielectrics

There exist 32 crystallographic point groups in nature that describe all crystalline materials based on symmetry operations. Dielectrics can be classified based on their point groups and polarity, among other physical features as introduced in Fig. 2.3.

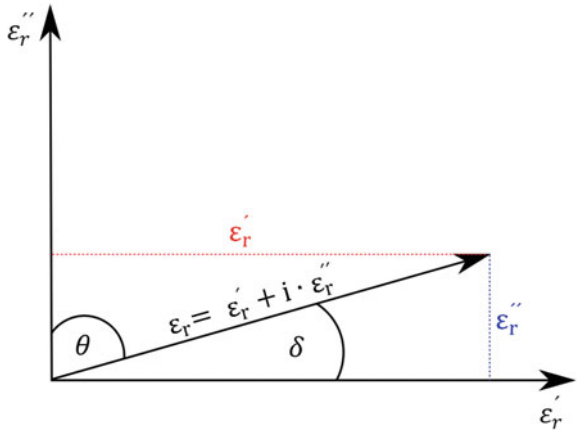

Fig. 2.2 Representation of ε_r in the complex plane. The real part of the relative permittivity is indicated by ε_r' and the imaginary part by ε_r''

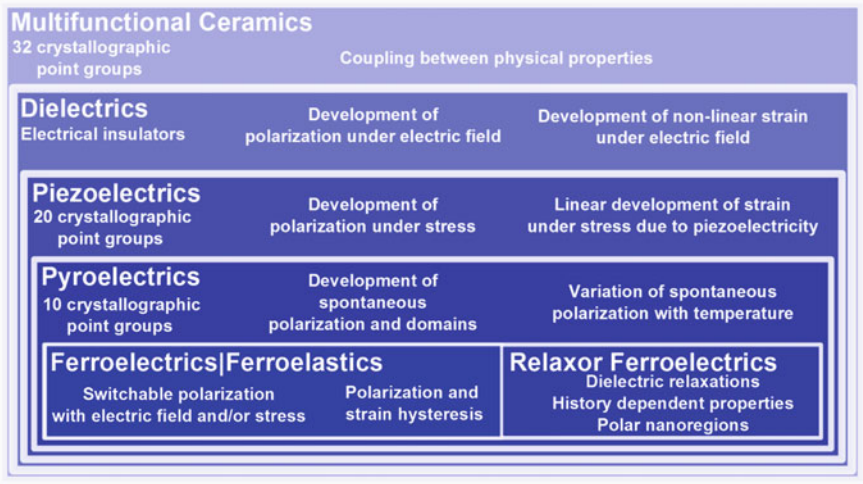

Fig. 2.3 Multifunctional ceramics classification indicating the subclasses of dielectrics found in nature and their respective physical features. To allow proper visualization, some classes of dielectrics like flexoelectrics and rotostrictors are not displayed in the image

Table 2.1 introduces the 32 crystallographic point groups and their classification according to symmetry considerations. As discussed in Sect. 2.1, application of an electric field to dielectrics will lead to an induced P_i and non-linear S_{ij}. From the aforementioned 32 crystallographic point groups, 11 are centrosymmetric due to the presence of a center of inversion. In these crystallographic point groups, odd couplings between S_{ij} and any other order parameter is forbidden due to symmetry reasons, according to Neumann's principle.

Table 2.1 Crystallographic point groups classification according to symmetry considerations

Crystal system	Centrosymmetric point groups	Non-centrosymmetric point groups	
	Non-Polar		Polar
Cubic	$m\bar{3}m, m\bar{3}$	$432, \bar{4}3m, 23$	–
Hexagonal	$6/mmm, 6/m$	$622, \bar{6}m2, \bar{6}$	$6mmm, 6$
Trigonal	$\bar{3}m, \bar{3}$	32	$3m, 3$
Tetragonal	$4/mmm, 4/m$	$422, \bar{4}2m, \bar{4}$	$4mm, 4$
Orthorhombic	mmm	222	$mm2$
Monoclinic	$2/m$	–	$2, m$
Triclinic	$\bar{1}$	–	1
Total	11	11	10

Notation is given according to Hermann-Mauguin notation

The 21 remaining point groups, except the point group 432,[3] depict at least one non-vanishing coupling coefficient between the order parameters P_i and S_{ij}. Therefore, non-centrosymmetric materials from these 20 final point groups will develop D_i (or in analogy P_i) when subjected to σ_{ij}, which is a conjugate thermodynamic variable of S_{ij} and thus also of D_i. The reversible and linear coupling between the order parameter D_i and the conjugate variable σ_{ij} under constant E_i and temperature introduced in Eq. 2.9 defines a piezoelectric material. Since the effect is linear, any change of σ_{ij} will result in a change of D_i.

$$D_i = d_{ijk}\sigma_{jk}, \tag{2.9}$$

where d_{ijk} is the direct piezoelectric coefficient. It should be noted that the couplings described for dielectrics in Eq. 2.5 will also result in D_i in a piezoelectric, for the case where the material is subjected to the described conjugate thermodynamic variables. The converse piezoelectric effect is defined as the linear change of S_{ij} that develops with application of E_k under constant σ_{ij} and temperature, as depicted in Eq. 2.10.

$$S_{ij} = d_{ijk}E_k, \tag{2.10}$$

where d_{ijk} is the indirect piezoelectric coefficient that is numerically identical to the direct piezoelectric coefficient. As with the direct effect, the converse effects described for dielectrics (Eq. 2.6) also contribute to S_{ij} in piezoelectrics. The efficiency of the piezoelectric effect on a given material can be determined by the

[3]The point group 432 is the only group with both a 4-fold and a 3-fold rotation axes. The 4-fold rotation axis leaves seven of the piezoelectric coefficients non-zero, and the 3-fold axis vanishes these coefficients leading to no coupling between D_i and σ_{ij}.

electromechanical coupling factor k. This parameter indicates the electrical energy converted into mechanical energy, as given in Eq. 2.11.

$$k^2 = \frac{electrical/mechanical\ energy\ converted\ into\ mechanical/electrical\ energy}{input\ electrical/mechanical\ energy}. \tag{2.11}$$

Another subdivision of piezoelectrics can be made analyzing the 20 remaining crystallographic point groups. From them, 10 possess a polar axis (i.e., a dipole moment) without being subjected to any conjugate thermodynamic variable and thus they display a non-zero P_i (or in analogy D_i) normally denominated spontaneous polarization P_s^i. Uniform changes in the conjugate thermodynamic variable temperature T will result in a change of P_s (note that upper script is avoided intentionally to indicate the norm of the tensor). These types of materials are known as pyroelectrics. Equation 2.12 introduces the definition of the direct pyroelectric coefficient pc_i.

$$pc_i = \frac{\partial P_i}{\partial T}. \tag{2.12}$$

Note that all polarization and strain mechanisms described for dielectrics and piezoelectrics also hold for pyroelectrics. Although pyroelectrics feature a polar axis, families of crystallographically equivalent orientations are allowed by symmetry in the ten pyroelectric point groups. The crystallographically and energetically equivalent orientations, as well as the need to minimize electrostatic energy, leads to the formation of regions in the material with the same spatial orientation of the P_s^i denominated domains. These regions are separated by domain wall boundaries. The interface charge density γ accumulated at the interface between two domains is described by Eq. 2.13.

$$\gamma = \left(P_i^1 - P_i^2\right) \cdot \hat{n} = \left\|P_i^1\right\| cos(\vartheta) - \left\|P_i^2\right\| cos(\vartheta), \tag{2.13}$$

where P_i^1 and P_i^2 indicate the polarization of both domains, $\hat{n}$ is the unit vector normal to the interface, and ϑ the angle between domain interfaces. Any domain configuration will lead to charged domain interfaces with the exception of two cases [34]. The surface charge will be zero for the case of antiparallel domains if $\left\|P_i^1\right\| \equiv \left\|P_i^2\right\|$ or for the case that the domain interfaces are orthogonal. The former case is generally denominated 180°-domain walls, while the latter non-180° domain walls (or 90° domain walls for the tetragonal phase). Domain arrangements generally have a mirror followed by a center of inversion, and thus arrange themselves as twin structures "head-to-tail" in space to avoid discontinuity of polarization at the interface [35, 36]. Figure 2.4 introduces a pyroelectric material with (a) 180°-domain walls, (b) non-180° domain walls, and (c) both domain configurations.

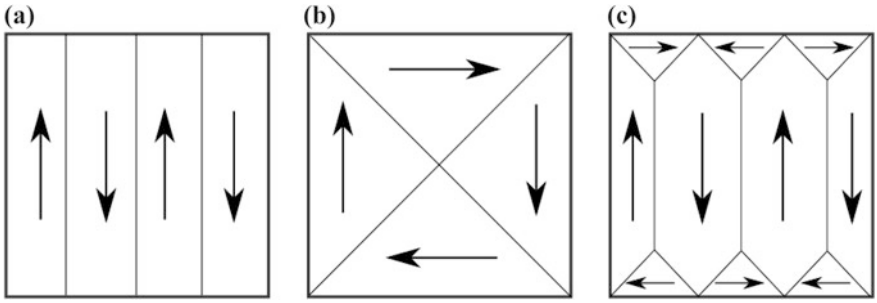

Fig. 2.4 Domain patterns for pyroelectrics and ferroelectrics. **a** Ferroelectric, **b** ferroelastic, and **c** polydomain patterns

Since the order parameters D_i and S_{ij} in pyroelectrics are coupled, the formation of non-180° ferroelastic domains builds up stresses. For this reason, the schematic representation introduced in Fig. 2.4b is rarely encountered. The state with 180° domain walls (Fig. 2.4a) typically forms in strain-free states. These domains characterize single crystals or coarse grain materials [37]. In most polycrystalline materials, however, the grains are in a clamped state due to the interactions between randomly oriented grains, and therefore the situation in Fig. 2.4c is generally favored. Although the energy of the polarized ground state is lost during domain formation, their presence compensates the electrical stray field energy caused by free charges and defects (Eq. 2.1). The energy gained is also compensated by domain wall formation and strain fields.

By definition, it is not possible to reorient P_s^i of domains in pyroelectrics. Therefore, a pyroelectric material will only develop a macroscopic measurable pc_i if domains within the material are arranged such that a non-zero macroscopic P_s^i is developed. Ferroelectric and ferroelastic materials are a subgroup of pyroelectrics that also feature a P_s^i and domains. They are unique since their domains can be reoriented between equivalent crystallographic orientations by conjugate thermodynamic variables such as E_i or σ_{ij}. Relaxor ferroelectrics are a subclass of ferroelectrics with complex structure and properties that depend on history and observation time. Therefore, frequency-dependent relaxation effects are common in these materials. Moreover, in most cases, they feature polar nanoregions (PNRs) [38] instead of domains. Ferroelectrics and relaxor ferroelectrics will be treated in the subsequent sections separately in detail due to their relevance to this work.

2.2.1 Ferroelectrics

Since the discovery of ferroelectricity in the single crystal Rochelle salt in 1921 [39] and polycrystalline ceramics during the 1940s [40–42], there has been a continuous succession of new materials and related technological developments. Appearance of

a P_s^i in ferroelectrics is a consequence of a structural change that breaks the center of symmetry of points groups. These structural changes are normally termed phase transitions and can be of first or second order. First order phase transitions are characterized by discontinuous changes in physical properties such as enthalpy corresponding to the evolution of latent heat of the transformation. This leads to thermal hysteresis in functional properties during phase transformation. Second order phase transitions are characterized by a continuous change of enthalpy and thus no latent heat is observed for these transformations. Either first or second order phase transitions can develop as order-disorder or displacive. In general, the former implies an ordering process while the latter refers to short-range displacements of atoms. Any of the phase transitions described may be responsible for lowering the symmetry of the high temperature point group in ferroelectrics. The phase transition and formation of a P_s^i occurs at the Curie temperature T_C and is accompanied by an anomaly in the temperature dependence of permittivity ε, as displayed in Fig. 2.5 for a first order phase transition (black) and for a second order phase transition (red).

The high temperature ε above T_C can be described by the Curie-Weiss law given in Eq. 2.14.

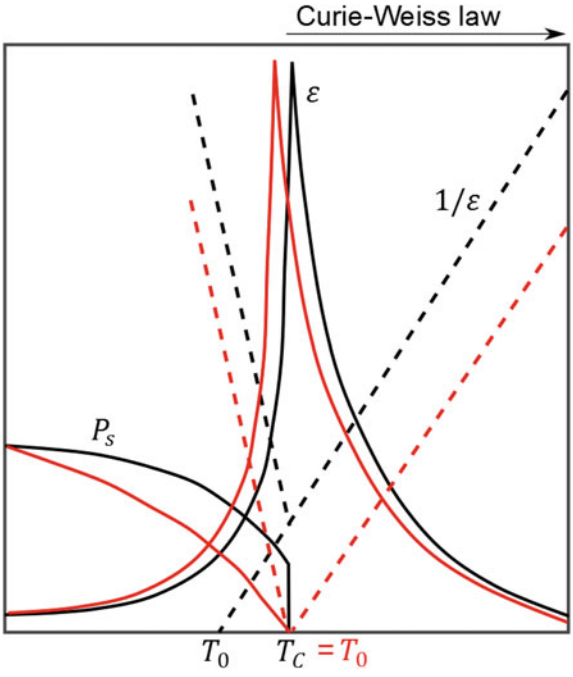

Fig. 2.5 Schematic representation of ε, $1/\varepsilon$, and P_s as a function of temperature for a ferroelectric. *Black lines* indicate a first order phase transition from the paraelectric to the ferroelectric state. If $T_C = T_0$, the phase transition is of second order (marked in *red*)

$$\varepsilon = \varepsilon_0 + \frac{C}{T - T_0} \approx \frac{C}{T - T_0}, \tag{2.14}$$

where C is the Curie constant and T_0 is the Curie-Weiss temperature, which is obtained by extrapolating the trend of the high temperature $1/\varepsilon$ data to its intersection with the abscissa axis. Only for second order phase transitions $T_0 = T_C$. Note that P_s and P_r vanish at T_C discontinuously for a first order phase transition or continuously in the case of a second order phase transition.

Ferroelectrics can be categorized into four groups: (1) pyrochlore group ($A_2B_2X_6$ or $A_2B_2X_7$), (2) tetragonal tungsten bronze group ($A1_2A2_4C_4B1_2B2_8X_{30}$), (3) bismuth-layer structure group ($A_{n-1}B_nX_{3n+1}$), and (4) octahedral group (ABX_3). The latter group, often simply called the perovskite group (due to the mineral perovskite $CaTiO_3$), is by far the most technologically relevant category and focus of this work. Figure 2.6 introduces the sequence of phase transitions featured in perovskite ferroelectrics such as for instance in the prototypical barium titanate, $BaTiO_3$ (BT) [43]. The high temperature prototype cubic structure (C) has a $Pm\bar{3}m$ space group. It is observed that the A-site cation has a 12-fold coordination, while the B-site cation has a 6-fold coordination. The generic X term is typically associated with an O^{2-} anion that is coordinated with 4 A-site cations and 2 B-site cations.

The distortions of perovskites are related to the structural frustration of the cubic structure. Due to structural and energetic considerations, the ferrodistortive (FD) distortions leading to ferroelectricity (Fig. 2.6) compete energetically with octahedral distortions [44]. The latter involve rigid rotations or tilting of octahedra and are known as antiferrodistortive distortions (AFD) since they may lead to antiferroelectricity. Goldschmidt developed an empirical criterion of stability for perovskite ferroelectrics, as given in Eq. 2.15. The tolerance factor t for ionic materials is based on a geometrical model that accounts for the filling of a unit cell by rigid spheres of radii r that represent ions.

$$t = \frac{r_A + r_x}{\sqrt{2}(r_B + r_x)}. \tag{2.15}$$

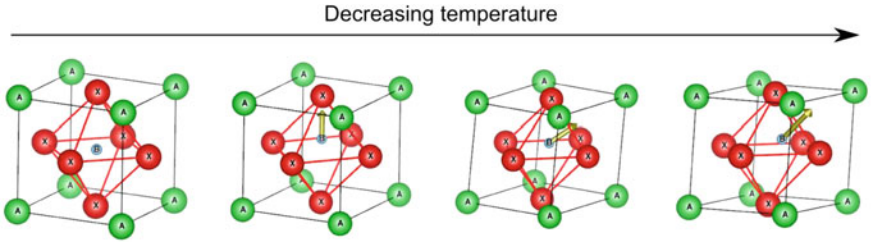

Fig. 2.6 Unit cells of a perovskite structure ABX_3. Octahedra of X anions are depicted in *red*, while *arrows* indicate P_s^i. With decreasing temperature, the prototypical cubic perovskite structure distorts to tetragonal, then orthorhombic, and finally rhombohedral phase

For $t \approx 1$ cubic perovskite structures are energetically favored. For $t > 1$, the cation on the B-site is small relative to the X octahedra, indicating that the structure will develop a polar distortion through displacement of the B-site cation. Conversely, for $t < 1$ the A-site cation is small relative to the center of the X octahedra, leading to a weakened bond between A-site cations and X-site anions. This gives rise to distortions of the X octahedra, such as rigid rotations or tilting. It should be noted that this empirical model neglects the degree of covalence of the bonds that also partially determines the preferred distortion [44]. The competing FD and AFD mechanisms responsible of ferroelectricity lead to a further classification of phase transitions. Octahedral distortions will result in formation of crystallographic structures that are modulated and give rise to incommensurate transitions. These transitions indicate that the periodicity of the forming phase is incommensurate with respect to the principal periodicity of the host lattice and leads to the presence of superlattice reflections (SSR) in diffraction patterns. In contrast, if the periodicity of the phase coincides with that of the host lattice phase, the phase transition is commensurate.

In the schematic view of Fig. 2.6, decreasing temperature below T_C can lead to the formation of a non-centrosymmetric tetragonal phase (T). In general, this phase is characterized by a *P*4*mm* (commensurate) or *P*4*bm* (incommensurate, not shown) space group. In this case a non-zero P_s^i develops along one of the six crystallographic directions of the $\langle 00l \rangle$ family. Further cooling leads to the formation of an orthorhombic phase (O) with the space group *Amm*2 and P_s^i along one of the 12 crystallographically equivalent $\langle hh0 \rangle$ family of directions. Subsequently, at even lower temperatures, a rhombohedral phase (R) develops with symmetry *R*3*c* and P_s^i along one of the eight equivalent $\langle hhh \rangle$ directions. Domain formation is common to all ferroelectrics upon development of P_s^i due to the energetic considerations treated in Sect. 2.2. One of the fundamental properties of ferroelectrics and ferroelastics is the ability to reorient their P_s^i by the application of E_i or σ_{ij} and thus a net macroscopic P_s^i can develop due to domain reorientation. A domain reorientation by either application of E_i or σ_{ij} is normally called a switching process and is understood as an extrinsic phenomenon, in contrast to P_s^i reorientation which is an intrinsic phenomenon. Domain switching is considered extrinsic because it is a process that takes place on a scale larger than the unit cell and requires the growing or shrinking of domains through motion of the domain walls. Two extrinsic effects have to be distinguished, since during the application of E_i, domain walls move reversibly or irreversibly in the local potential generated by the interaction between lattice, defects, and domain walls. A schematic representation of this process is displayed in Fig. 2.7. Reversible domain wall movements are due to displacement of the domain wall from its local minimum, while irreversible movements can be regarded as jumps above a potential barrier into other local minima.

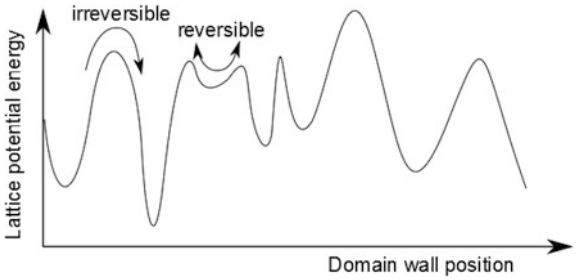

Fig. 2.7 Scheme of domain wall displacements in the lattice potential

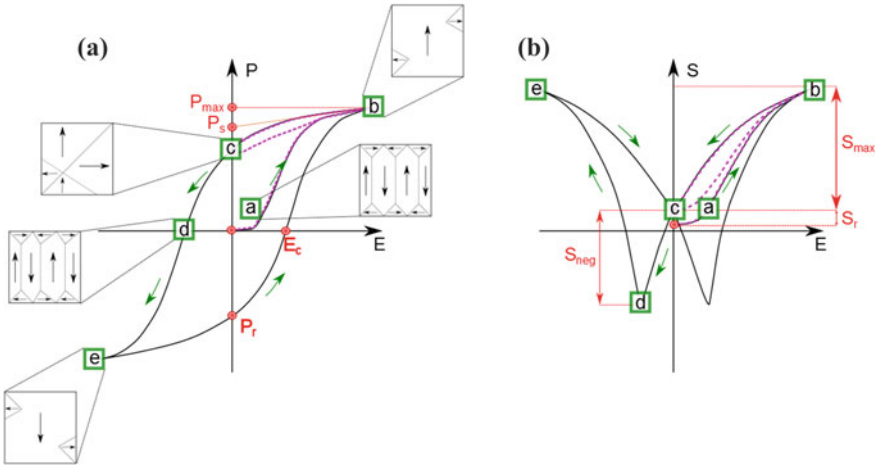

Fig. 2.8 **a** Schematic bipolar polarization and **b** bipolar strain loops of a ferroelectric. Relevant parameters for the characterization of ferroelectrics are marked, together with a scheme of the domain patterns expected at each point of the loop. The unipolar strain and polarization loops are also depicted in (**a**) and (**b**) with *dashed purple lines*, respectively

Extrinsic contributions lead to the characteristic polarization and strain hysteresis loops in ferroelectrics. Figure 2.8a and b introduce the prototypical bipolar polarization and strain hysteresis loops measured in the 333 mode,[4] respectively. Solid lines indicate the bipolar loops, while dashed lines the unipolar loops.

The virgin domain state is generally determined by a complex energy interaction between electrostatic and elastic energy, as described in Sect. 2.2. The domain patterns associated with different points of the polarization and strain hysteresis loops are displayed schematically. At point ⓓ in Fig. 2.8, a virgin state characterized by a random polydomain pattern with 180° and non-180° domains leading

[4]The 333 mode describes the polarization and strain response of a sample poled in the measurement direction.

to negligible macroscopic P_s^i is displayed. Note that point [a] is at higher electric field strength that the onset required to obtain macroscopic properties, however, the electric field strength is not high enough to promote appreciable irreversible domain wall motion. However, non-linearity may be present at low electric fields and is ascribed to reversible domain wall motion [45]. Nevertheless, at this electric field polarization and strain are approximately linear and reversible mostly due to direct and converse piezoelectricity, electrostriction, as well as plausibly due to roto-striction, and flexoelectricity. The slope of the strain curve at this point is equal to d_{333}. From now on, Voigt notation is considered and the piezoelectric coefficient will be referred to as d_{33}. As the electric field strength is increased, domains start to align in the positive direction due to reversible and irreversible switching. This gives rise to a rapid increase in both polarization due to non-180° and 180° domain switching, as well as in strain mostly due to non-180° switching. At any given electric field strength, where strain output deviates considerably from linearity, a large signal piezoelectric coefficient can be defined as in Eq. 2.16.

$$d_{33}^{*} = \frac{S_{33}}{E_3}. \tag{2.16}$$

The small signal d_{33} and large signal d_{33}^{*} are normally considered as figures of merit for actuator applications. Once domain switching saturates at point [b], further increase in applied electric field activates only an intrinsic response leading to a linear increase in polarization and strain similar as at point [a]. The saturated domain state achievable generally does not result in a monodomain state due to the random orientations of grains inherent to polycrystalline ceramics, but even in single crystals there is stray energy, defects and/or stresses that must be taken into account. The maximum polarization P_{max} and maximum strain S_{max} could, but do not necessarily always, indicate saturation values. The latter term is generally an indication that a maximum domain orientation was achieved leading to a purely linear response. Once the electric field is removed, domains will partially switch back to the crystallographically allowed orientations at point [c]. The lattice intrinsic response may not be fully reversible and a number of 180° and non-180° domains will remain oriented with the previously applied electric field direction, indicating irreversible switching. Therefore, intrinsic and irreversible extrinsic switching leads to a non-zero remanent polarization P_r and remanent strain S_r. The remanent state is normally termed a poled state since it features a non-zero macroscopic P_s^i due to a preferred domain alignment direction. The P_s can be estimated by extrapolating the linear polarization region near P_{max} to zero applied electric field along the saturated polarization tangent. If an electric field with an opposite polarity to the initial poling field is applied to the material, it will promote switching along this new direction. Once the electric field reaches a magnitude equal to the coercive field E_c, the material's P_s will vanish. This is achieved by establishing a random domain state (point [d]) that does not necessarily coincide with the virgin state (point [a]). Therefore, the E_c can be regarded as the macroscopic electric field indicative of

switching processes. However, as previously stated, switching can occur at electric fields much lower than E_c [46]. The polarization decrease from point [c] to point [d] will be directly reflected in a compression of the material leading to a "negative strain" S_{neg}. This is a result of the compression experienced by domains opposed to the electric field direction at point [d] prior to switching. Further increase of the electric field results in the development of a P_{max} and S_{max} with an opposite polarity to the first half-cycle. Decreasing the electric field back to zero results in a remanent state characterized by a P_r and S_r, also with opposite polarity compared to the first half-cycle. Further electric field cycles retrace the path described from point [b] to point [e] leading to a continuous hysteresis. Point [a] will only be achieved again if the ferroelectric is depolarized to its virgin state by annealing it above T_C. The process described will not vary considerably at different temperatures if the ferroelectric state is conserved. In general, increasing temperature will decrease the E_c due to enhanced domain switching, which is logical considering that this process is thermally activated [47]. Above T_C, hysteresis will disappear and the dielectric will respond to the electric field, as described in Sect. 2.1. For unipolar electric field input, the purple unipolar polarization and strain hysteresis loops will be obtained leading to a hysteresis with the processes described from point [a] to point [c].

2.2.2 Relaxor Ferroelectrics

2.2.2.1 General Description

Relaxor ferroelectrics, often referred to as relaxors, exhibit complex physical features. These properties are the result of a chemically and/or structural disorder at the local scale, although they are generally represented in long-range analytical methods by a pseudocubic crystal structure. They have attracted considerable research attention due to their large responses to external stimuli [48]. Smolenskii et al. [49–51] reported the first relaxors during the 1950 and 1960 s. At high temperatures, perovskite relaxors depict a paraelectric cubic phase similar to that described for perovskite ferroelectrics (Fig. 2.6). However, upon cooling below the so called Burns temperature T_B they transform to an ergodic relaxor state with the presence of nanometer scale randomly oriented dipoles normally called polar nanoregions PNRs [38, 52, 53]. These PNRs can be regarded as clusters on the order of 10 nm composed of thermally activated dipolar entities that originate from local deviations in crystal structure and/or chemical heterogeneities in the A- and/or B-site cation sublattices [54–58]. Several attempts have been made to rationalize relaxors within one theoretical model. However, so far no general agreement in their microscopic picture has been achieved. The most widely accepted attempts capable of describing only some of their features are known as the diffuse phase transition model [50, 51], superparaelectric model [28], glassy state model [59–61], random fields model [62–65], spherical random bond-random field model [66–70], and breathing model [71,

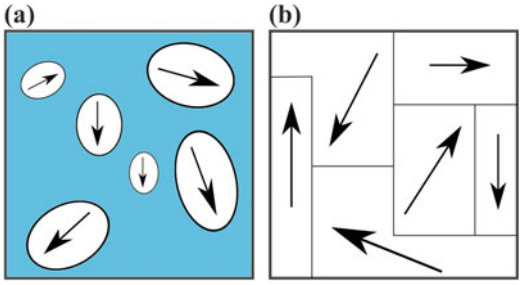

Fig. 2.9 Schematic representation of PNRs according to different models. Microscopic view (**a**) indicates a dipolar glass with embedded PNRs in a pseudocubic matrix, whereas (**b**) shows a frustrated ferroelectric with nanodomains due to the presence of random fields. *Arrows* are used to designate dipole moments

72]. These models can be categorized according to two microscopic views. Figure 2.9a displays PNRs embedded in a non-polar pseudocubic matrix and is supported by all models with the exception of the random fields model that describes relaxors as a frustrated ferroelectric state with nanodomains (Fig. 2.9b).

The high temperature state of relaxors, just below T_B, was named an ergodic state due to its similarity to the ergodicity term from statistical mechanics. An ergodic property or state is when the time average characteristic of the property is indistinguishable from the ensemble average for the distribution of all accessible points in the phase space of the system. In other words, in an ergodic system an arbitrary function can be defined in a certain mathematical space within the phase space of the whole system, in which the characteristic property's time average becomes indistinguishable from the ensemble over all accessible points [73, 74]. Expressing a higher degree of ergodicity can be understood as increasing the fraction of phase space in which its property time average characteristic becomes indistinguishable from the ensemble average for the distribution of all accessible points in the phase space of the system. Expressing a degree of non-ergodicity within a phase space is therefore not proper but a consequence of the degree of ergodicity. In this context, the ergodic state of relaxors can be understood as a state in which the polarization of uncorrelated PNRs has an equal probability of being found in any direction and at any point of the material. Therefore, ergodic relaxor can be distinguished from ferroelectrics based on their polarization. Ferroelectrics feature a non-zero value of P_s^i along crystallographically allowed orientations as indicated by $\sum_i P_s^i \neq 0, \sum_i \left\|P_s^i\right\|^2 \neq 0$. In contrast, relaxor materials have zero macroscopic P_s^i values but their quadratic contribution is non-zero due to the presence of PNRs $\sum_i P_s^i = 0, \sum_i \left\|P_s^i\right\|^2 \neq 0$. Characterization of physical features that depend on $\left\|P_s^i\right\|^2$ such as refractive index can be used to corroborate the presence of PNRs [52, 53]. On further cooling, different situations arise depending if the relaxor is canonical or non-canonical, as depicted in Fig. 2.10.

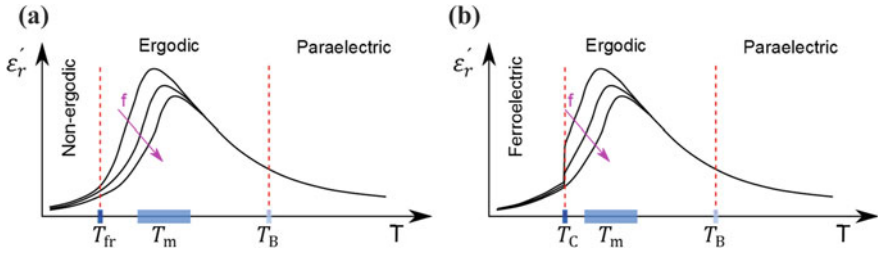

Fig. 2.10 **a** Prototypical ε_r' for canonical relaxors. **b** Prototypical ε_r' for non-canonical relaxors. Increasing measurement frequency is displayed with a *purple arrow*

Figure 2.10a represents a canonical relaxor that features a dynamic slowing down or relaxation of the PNRs fluctuations giving rise to a frequency-dependent maximum of ε_r' (as well as ε_r'', not displayed in Fig. 2.10). The temperature corresponding to the highest magnitude of ε_r' is normally defined as T_m and is a result of a dielectric relaxation. Cooling below T_m does not lead to changes of the average long-range cubic phase [29]. With further cooling, the PNRs of canonical relaxors become frozen leading to a glassy non-ergodic state at the freezing temperature T_{fr}. The concept of a T_{fr} was previously coined for spin glasses. These magnetic materials are characterized by localized interacting magnetic moments [75]. The T_{fr} represents a magnetic relaxation that can be determined from the frequency dependence of the susceptibility which approaches a constant value at lower frequencies [59]. This magnetic relaxation can be described by a relationship attributed to Vogel [76] and Fulcher [77] as defined in Eq. 2.17.

$$\omega = \omega_0 e^{\frac{-E_a}{k(T_m - T_{fr})}}, \tag{2.17}$$

where ω is the frequency of the relaxation process, E_a is the activation energy, ω_0 is the Debye frequency, and k is the Boltzmann constant. The Vogel-Fulcher relationship may be interpreted as a Debye relaxation with a temperature-dependent activation energy, which increases as the temperature decreases and becomes undefined at T_{fr} [59]. When Viehland et al. [59] first demonstrated that the Vogel-Fulcher relationship is applicable to relaxor ferroelectrics, this led to the categorization of these materials as dipolar glasses. Dipolar glasses differ from spin glasses in that they depict long-range dipolar interactions and non-negligible coupling of dipolar and structural degrees of freedom [64]. For the case of relaxors, the Vogel-Fulcher entails a temperature-dependent correlation length of PNRs. The divergence of the PNRs correlation length leads to divergence of their relaxation time and to a frozen state at T_{fr} [78, 79]. This state is characterized by distinct history-dependent functional properties [30, 60], as a result of the multiple metastable states of canonical relaxors in their non-ergodic state [74]. Non-canonical relaxors feature an analogous high temperature paraelectric and ergodic state when

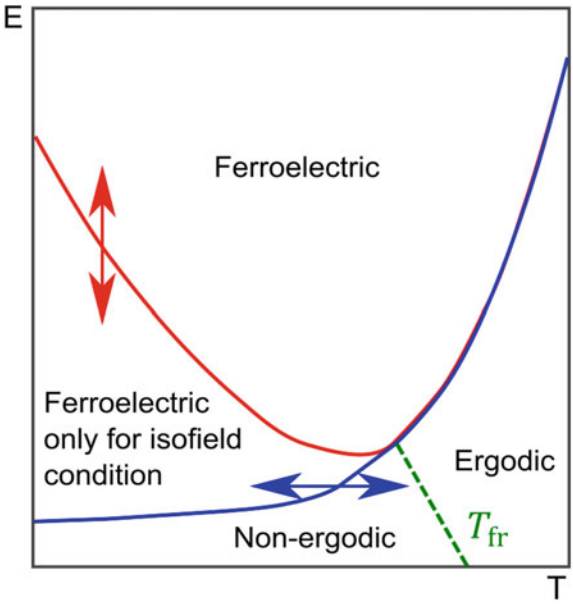

Fig. 2.11 Schematic representation of temperature and electric field evolution of canonical relaxors. *Red line* indicates isothermal conditions, *while blue line* isofield conditions

compared to canonical relaxors, as displayed in Fig. 2.10b. Upon further decrease in temperature below T_m, however, they have a spontaneous transition into a ferroelectric state. The temperature corresponding to this spontaneous transformation may be termed T_C since upon crossing this temperature the value of their macroscopic P_s^i vanishes. Only canonical relaxors will be further analyzed due to their relevance to this work.

As schematically shown in Fig. 2.11, applying an electric field of sufficient magnitude in both ergodic and non-ergodic states may induce a long-range ferroelectric state [80]. It should be noted that due to the history-dependent properties in the non-ergodic state of canonical relaxors [74], isothermal (red) and isofield (blue) representations differ [80, 81]. An electric field induced phase transition that originates from an ergodic state will be reversible, whereas from a non-ergodic state (below T_{fr}) will be irreversible. Increasing temperature without an external electric field destabilizes the induced ferroelectric state. The depolarization temperature T_d indicates the detexturization of ferroelectric domains and as a consequence is accompanied by the decay of macroscopic piezoelectric properties. Decay of the detextured domains into PNRs occurs at the ferroelectric to relaxor phase transition temperature T_{f-r} [82, 83].

One of the most important properties of canonical relaxors is that upon application of an electric field they display a slim and/or pinched polarization hysteresis loop, as displayed in Fig. 2.12. Compared to ferroelectric materials (Fig. 2.8a), this loop is characterized by a considerably smaller P_r. Point [a] in Fig. 2.12 indicates

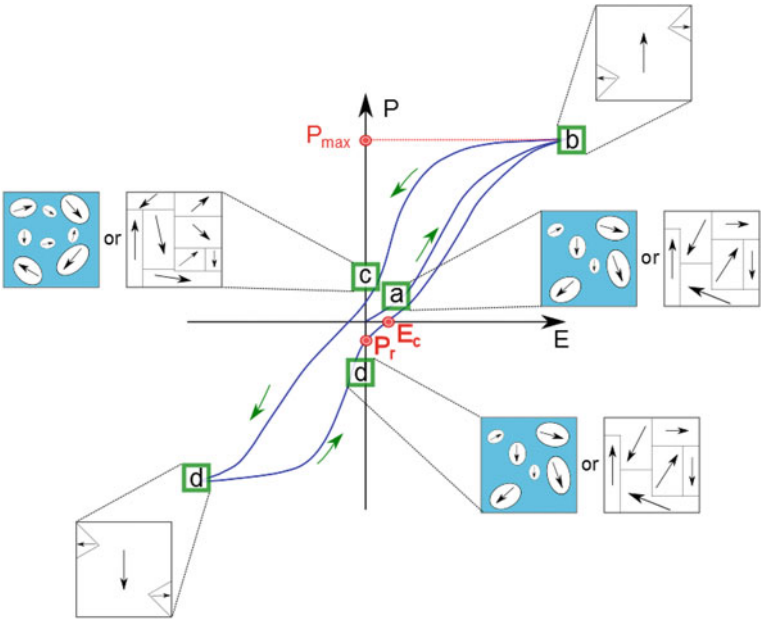

Fig. 2.12 Relaxor bipolar polarization loop and prototypical microscopic relaxor views for different electric field strengths

that the electric field strength is not high enough to induce a long-range ferroelectric state. Increasing further the applied electric field, however, induces a ferroelectric state along its direction (point $\boxed{b}$). Reduction of the electric field leads to the partial decay of the ferroelectric state in a material with a certain degree of ergodicity (point $\boxed{c}$) or to a random ergodic relaxor state with negligible macroscopic P_s and P_r. Increasing electric field with an opposite polarity to the first half-cycle leads to the same processes previously described (points $\boxed{d}$ and $\boxed{e}$). Further electric field cycles retrace the path from point $\boxed{b}$ to point $\boxed{e}$ leading to a continuous hysteresis. The induced ferroelectricity depicts similarities with a normal ferroelectric state in the sense that the material features a polarization loop attributed to some degree of interactions of PNRs. However, in the case of an ergodic relaxor the points $\boxed{a}$, $\boxed{c}$, and $\boxed{d}$ are indistinguishable. Relaxors feature generally large electrostrictive coefficients and therefore high electric field induced strains, which makes them technologically relevant for actuator applications [29, 84, 85]. Since both polarization and electrostriction are induced by the electric field, increasing temperature leads to diminished outputs [86].

Figure 2.13 introduces the thermal evolution of the P_s values for a ferroelectric with a first order phase transition (black), a second order phase transition (red), and a canonical relaxor with certain degree of non-ergodicity (blue). Since polarization in relaxors is ascribed to PNRs, it persists up to T_B [52, 53]. Note that for both

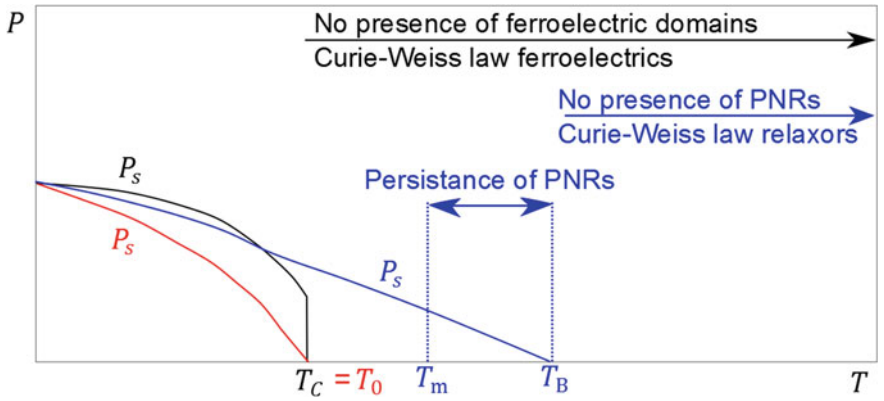

Fig. 2.13 Comparison of polarization decay with increasing temperature for a ferroelectric with first order phase transition (*black*), second order phase transition (*red*), and relaxor (*blue*)

canonical and non-canonical relaxors the Curie-Weiss law holds only for temperatures above T_B [87].

2.2.2.2 Lead-Free Relaxor Ferroelectrics

The exact nature of the relaxor state in lead-free perovskites remains an active matter of debate within the research community. Lead-free perovskite relaxors can be considered as materials with a quasi-continuous order parameter in 3 dimensions, which leads to 3 dimensional PNRs, similarly to those found in lead-containing perovskite relaxors. Both the Aurivillius and tetragonal tungsten bronze lead-free relaxor systems depict 2 and 1 dimensional order parameters with PNRs of the same dimensionalities, respectively. The general features of lead-containing canonical relaxors introduced previously are also observed in lead-free relaxors. However, some more complex physical phenomena have also been observed:

- In contrast to lead-containing materials, in which relaxor properties are observed for heterovalent A- or B-site modified materials (e.g. $Pb(Mg_{1/3}Nb_{2/3})O_3$), lead-free relaxors are found in both homovalent and heterovalent A- and B-site modified materials, such as BT with Zr^{4+}, Ca^{2+}, Na^{+}, Nb^{5+}, among many others [88–90].
- An average long-range pseudocubic structure is not always observed in lead-free relaxors [91].
- Local antiferroelectric PNRs were proposed [92].
- A distribution in the degree of ergodicity may develop locally, which could be ascribed to different coexisting symmetries of PNRs [93].
- Temperature insensitive electrostrictive strain output was discovered in some materials [94].

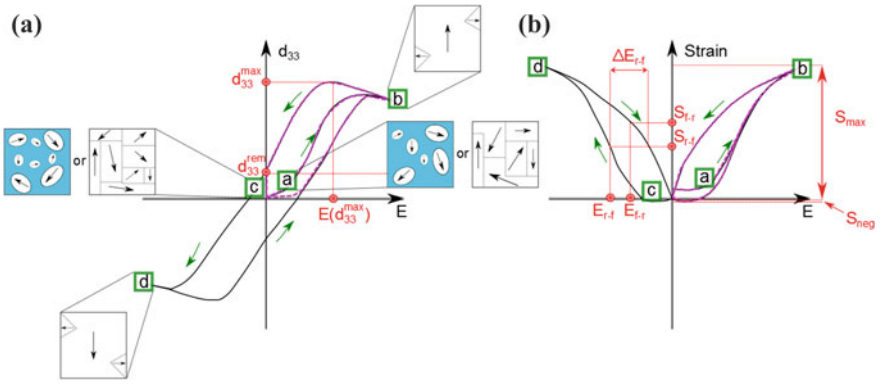

Fig. 2.14 Schematic curves of **a** d_{33} and **b** bipolar (*solid black line*) and unipolar (*dashed purple line*) strain output of incipient piezoelectrics as a function of electric field. Prototypical microscopic relaxor views for different electric field strengths are also displayed

One of the most thoroughly investigated class of lead-free relaxors are BNT-based incipient piezoelectrics. Incipient piezoelectrics can be defined as materials that possess a destabilized ferroelectric state achieved by the addition of chemical dopants or modifiers. The term incipient denotes "beginning to happen or develop". This indicates that at zero bias-field these materials depict an ergodic relaxor state with negligible d_{33}, whereas under electric field they develop a ferroelectric state and a reversible induced giant strain [95–113] and d_{33} values [95], as schematically introduced in Fig. 2.14. Research on these materials has focused on understanding their strain mechanism in order to further enhance it. The origin of the large electromechanical response of incipient piezoelectrics is generally attributed to an electric field induced phase transition [114–121].

Figure 2.14 at point [a] displays an ergodic relaxor state, as previously discussed. For BNT-based lead-free incipient piezoelectrics, it was demonstrated that the electric field induced phase transition coincides with the inflection point of the strain output [122] and the transformation is followed by switching of the newly created domains [117, 118]. Note that the inflection point of the strain curve also coincides with increased polarization [122]. Both processes lead to maximized d_{33} values (i.e., d_{33}^{max}) and a maximized $\frac{\partial S_{33}}{\partial E_3} = S_{r-f}$ [95, 123]. Therefore, the inflection point of the strain curves indicate the electric field required to trigger the phase transition from the relaxor to the ferroelectric state at E_{r-f}. An electric field hysteresis ΔE_{r-f} is observed when the development and decay processes are compared [122]. Saturation of small and large signal electromechanical response is subsequently achieved, as displayed in point [b]. Upon removal of the electric field, the induced ferroelectric state decays into an ergodic state at E_{f-r} (point [c]) and is accompanied by a strain output with a value of S_{f-r}. When the electric field is removed, incipient piezoelectrics with a distribution of ergodicity may retain part of the induced ferroelectric state [93]. Prior to switching, the retained domains

contract, similarly as in ferroelectrics (Fig. 2.8 point [d]), leading to non-zero S_{neg}. Further electric field cycles retrace the response described resulting in hysteresis. Unipolar cycling will lead to the strain response displayed with dashed lines and a similar structural evolution as described for the bipolar case from points [a] to [c]. As it will be seen in Sect. 2.3, incipient piezoelectrics depict a giant strain output surpassing the strain of lead-containing and other lead-free materials. Thus they are especially relevant for applications such as actuators.

2.3 Electromechanical Enhancements in Ferroelectrics

The last seven decades of research on ferroelectrics yielded strategies to enhance strain mechanisms [124, 125], as displayed in Fig. 2.15. To date, compositional engineering remains the preferred approach, although structural engineering has also led to technologically relevant achievements [124]. The strategies in white modify both intrinsic and extrinsic contributions to the piezoelectric activity, while those in light blue modify mostly the extrinsic contributions. Note that other approaches not directly related to the modification of material parameters can also be employed to enhance electromechanical properties. External stimuli such as

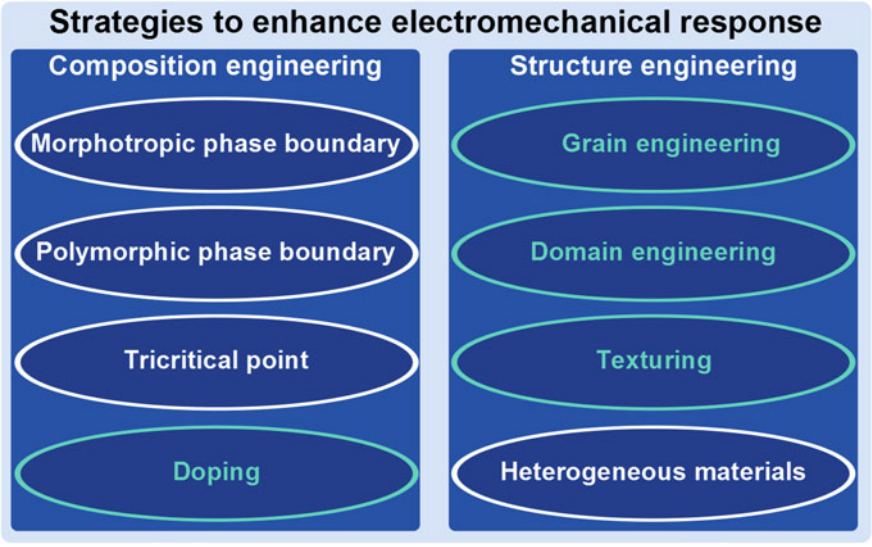

Fig. 2.15 Compositional and structural engineering strategies to optimize electromechanical response of ferroelectrics. Strategies in *white* are used to enhance both intrinsic and extrinsic contributions to the piezoelectric activity, while those in *light blue* mostly modify extrinsic contributions

optimization of the poling procedure through temperature or mechanical loading, as well as mechanical loading during service are also fruitful strategies. Nonetheless, they will not be treated in this work.

2.3.1 Composition Engineering

2.3.1.1 Phase Instabilities

It is well-known that dielectric and electromechanical properties are enhanced around phase instabilities [13]. Phase instability indicates that a material possesses polymorphism; i.e., it features two or more different crystal structures depending upon changes in composition and/or thermodynamic variables. In contrast, isomorphism is defined as the case where compounds possess the same crystal structure, although they have different chemical composition [126]. Goldschmidt [126] proposed a distinction between the compositionally-driven polymorphs from those that arise as a result of changes in thermodynamic variables. The former boundary indicating a compositionally-driven change in polymorph, was designated a morphotropic phase boundary (MPB). The latter boundary, occurring as a consequence of a change in thermodynamic variables and at constant chemical

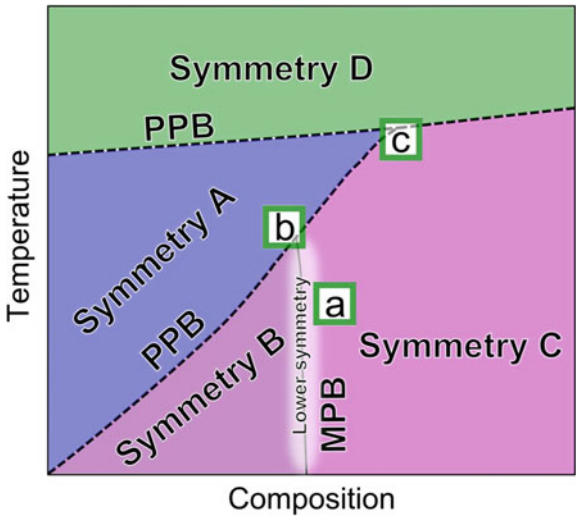

Fig. 2.16 Schematic composition-temperature phase diagram depicting five symmetries, two PPBs, and one MPB. The *white shaded* region indicates the presence of an average lower symmetry structure than symmetries B and C. The *dashed phase* boundaries indicate second order phase transitions, whereas the *solid line* represents a first order phase transition

composition, was denominated a polymorphic phase boundary (PPB). It must be pointed out, however, that the term MPB has also been employed in several occasions in the ferroelectrics community to indicate an increased multiplicity of polarization states contributing to enhanced electromechanical properties [127]. Figure 2.16 displays a schematic of a composition-temperature phase diagram representing MPBs and PPBs in ferroelectrics. The presence of five symmetries and three phase boundaries is depicted. Second order phase transitions are indicated by dashed lines, while the solid line represents a first order phase transition.

Considerable research has been performed in BT-based materials or KNN-based materials characterized by presence of PPBs [20, 124, 128]. Alternatively, research has also focused considerably on systems with presence of a MPB-like[5] transition such as in lead-based piezoelectrics or in some BNT-based materials [20, 124, 125, 128–130]. The origin of maximized properties at interferroelectric phase boundaries has been commonly attributed to a FD transverse instability of P_s^i that ease its reorientation due to increased multiplicity of polarization states, reduced free energy anisotropy, and softening of the crystal lattice [13, 124, 131–135]. Transverse instabilities have been pointed out in several works as the key for the enhancement of dielectric and electromechanical properties [132, 134–142]. Based on the soft-mode theory of ferroelectricity [143], crystal softening is a result of an optical phonon that dramatically reduces its frequency down to zero during phase transitions. The disappearance of the phonon gives rise to the new symmetry and consequently enhances dielectric and piezoelectric properties. Moreover, crystal softening can further enhance extrinsic contributions due to intergranular stress accommodation [143]. These mechanisms seem to be common to all displacive interferroelectric phase boundaries [144]. For the case of a ferroelectric to paraelectric phase transition, an analogous phenomenon has been proposed. At this phase boundary a FD longitudinal instability favors the P_s^i contraction/extension [132, 144]. Figure 2.17 introduces the phase diagram of PZT and the free energy profiles calculated near phase boundaries. The dashed lines indicate easy paths for P_s^i to either rotate or extend and contract. The easy paths for P_s^i reorientation are determined by a minimization in free energy anisotropy (i.e., the free energy surface is flattened giving a lower energy barrier for P_s^i to change its spatial direction). Therefore, this rationalization of strain enhancements mostly deals with intrinsic contributions to the piezoelectric activity. Approaching T_C to maximize the polarization extension contribution is not a convenient strategy due to the inherent reduced temperature stability of this enhancement. In order to develop technologically relevant materials using the longitudinal instability of P_s^i approach, the development of a temperature insensitive phase boundary between a polar phase and a non-polar phase is necessary [144]. This prospect was raised during the research of the mechanisms responsible for incipient piezoelectricity discussed in Sect. 2.2.2.2, as they feature this type of instability. Irrespective of the type of

[5]To the best of the author´s knowledge, none of the phase boundaries known in ferroelectrics is strictly in accordance with the definition of an MPB proposed by Goldschmidt.

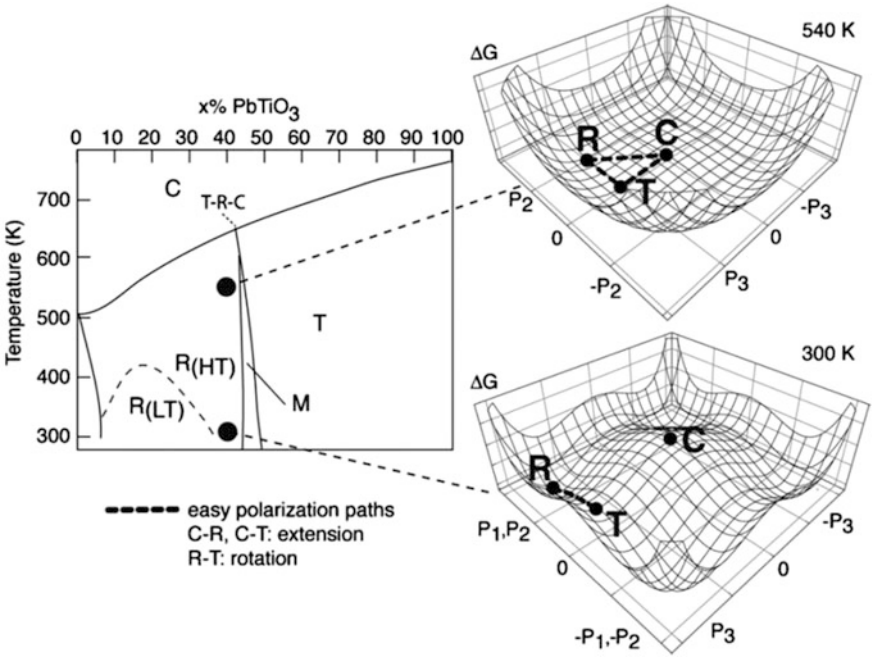

Fig. 2.17 Composition-temperature phase diagram of PZT and Gibbs free energy profiles calculated at 300 and 540 K with the phenomenological Landau-Ginsburg-Devonshire theory. *Black dots* in the phase diagram indicate the temperature at which energy profiles were calculated, while *black dots* on the energy profiles indicate the equilibrium phases. Lines between equilibrium phases indicate the easier polarization paths for phase transformation. *C* cubic phase, R_{HT} high temperature rhombohedral phase, R_{LT} low temperature rhombohedral phase, *M* monoclinic phase, *T* tetragonal phase. Reprinted with permission of Damjanovic [144] copyright (2015), AIP Publishing LLC

instability, systems with MPBs are preferred over those with PPBs. The technological advantage of an MPB over a PPB is that it enables temperature insensitive enhancement of electromechanical properties. Therefore, this phase boundary has traditionally been the focus of ferroelectrics development [124]. In general, it was pointed out that apart from the temperature insensitive electromechanical response, piezoelectric activity in materials with MPBs persists to higher temperatures than in materials with PPBs since any crossover of a phase boundary degrades piezoelectricity [124]. Retention of the P_r to higher temperatures in systems with MPBs can be attributed to a steeper free energy anisotropy reduction surrounding this phase boundary. In other words, the more tilted the PPB the more shallow the free energy profile becomes. This results in a reduced free energy anisotropy, which aids polarization mobility leading to a transverse instability of the P_s^i and thus lower retention of the P_r [131, 134, 136].

The MPB region marked with point ⓓ in Fig. 2.16 has been generically characterized as O or Monoclinic (M) phases [145–151]. This interleaving region was

proposed to be a bridge phase between the nearby phases B and C, as there is no group-subgroup relation between the commonly found $P4mm/P4bm$ and $R3c$ symmetries. It was stated that these phases aid P_s^i reorientation, indicating that this model mostly rationalizes intrinsic contributions. However, it has been pointed out that the M phase may be in fact composed of finely twinned R and T domains [153–155] or that its existance may only be metastable [149]. There have also been other mechanisms proposed in order to rationalize the extrinsic contributions to the electromechanical enhancement around MPBs. For instance, chemical ordering [156, 157], formation of nanodomains [149, 158, 159] with facilitated switching [160], and others have been invoked. However, even in the case of domain miniaturization, it has been pointed out that the most important factor to consider is the mobility of domains rather than their size [161].

The electromechanical enhancement around phase instabilities remains an open research area. It has been pointed out that reduced free energy anisotropy, crystal softening, nanodomain formation, local chemical/structural ordering, and local low symmetry phases may be in fact intrinsically related and the most fundamental reason behind strain enhancement a "matter of taste" as far as how it is described by a given scientist [151]. Damjanovic [132] highlighted that a structural instability is only a sufficient condition but not necessary for enhanced electromechanical properties, the crucial property for high piezoelectric activity is that the free energy instability leads to reduced free energy anisotropy. In fact, ferroelectric or ferroelastic domain switching is a result of a free energy instability achieved by an external electric field or stress, respectively. This in turn gives rise to the maximized changes of polarization and strain around E_c in ferroelectrics and around E_{r-f} in incipient piezoelectrics. In the case, where no electric field induced phase transition is observed, the drastic change of polarization and strain are due to a P_s^i instability in either the transverse (non-180° domain switching) or longitudinal (180° domain switching) sense. Nonetheless, switching remains an extrinsic effect and several factors other than lattice considerations should be examined in order to understand it [132, 162].

Some authors extended the concept of a free energy anisotropy further and evoked criticality as the fundamental reason behind enhanced properties [163–166]. A critical point is defined as a continuous transition from a first order to a second order phase transition under thermodynamic equilibrium that does not involve thermal hysteresis. Near these critical points, the energy barrier for a phase transition is considerably diminished. This indicates a more pronounced decrease of the free energy anisotropy and enhanced properties [10, 134, 167, 168]. It was pointed out that maximizing the number of coexisting phases near multicritical points leads to increased entropy and thus higher enhancement of electromechanical properties [167]. Point $\boxed{b}$ in Fig. 2.16 exemplifies both a triple point and critical point, since a first order phase transition (solid line) leads to a second order phase transition (dashed line) as the temperature is increased. In contrast, point $\boxed{c}$ in Fig. 2.16 displays a triple point with no criticality. It should be noted, however, that the triple point in Fig. 2.16 marked with $\boxed{b}$ is not necessarily a tricritical point. A tricritical

point, refers to the point where, at a fixed composition, the lines of critical points in the temperature-electric field-pressure phase diagram converge [10]. Therefore, their experimental determination is quite difficult [131]. The coincidence of a tricritical point with a triple point such as the one marked with [b] in Fig. 2.16, will only occur in the hypothetical case that the critical points in the temperature-electric field and electric field-pressure phase diagrams intersect at the same temperature-composition coordinates of the triple point (at zero electric field and atmospheric pressure). The exceptionally large electromechanical properties of some BT-based materials were previously attributed to the presence of tricritical points [169–171].

2.3.1.2 Doping

Ferroelectrics have also been traditionally engineered with isovalent or aliovalent dopants or modifiers to improve their functional properties for specific applications [19, 20]. Modifiers are used to engineer a composition in proximity to phase boundaries, as treated in the last section. Although dopant quantity may be very low, the functional properties of doped materials can vary drastically due to modification of the extrinsic contributions to the functional properties [18, 161, 172]. Aliovalent doping can be classified as donor or acceptor. Donor doping indicates that the oxidation state of the dopant is higher than the oxidation state of the host lattice site. In order to maintain charge neutrality, donor doping is compensated either by cation vacancy formation, decrease in oxygen vacancies, or electronic. Donor doped ferroelectrics are referred to as soft since they feature high dielectric and electromechanical properties, square ferroelectric hysteresis loops, and high dielectric loss. These properties are attributed to a high degree of switching that can contribute to more than 40 % to piezoelectric and dielectric properties [24, 161, 172]. Acceptor doping describes the situation where the dopant has a lower oxidation state than the host lattice site. In this case, doping is compensated by an increase in oxygen vacancies or holes. Acceptor doping can lead to the formation of defect dipole complexes between dopant ions and oxygen vacancies [173]. These materials are known as hard materials, since the interaction between defect dipole complexes and domains leads to decreased switching processes. Hard ferroelectrics generally have low dielectric and electromechanical properties, low dissipation factor, pinched ferroelectric hysteresis loops, and an internal bias-field [125].

2.3.2 Structure Engineering

2.3.2.1 Grain and Domain Engineering

Structure engineering is a feasible way to achieve enhanced properties via a modified processing route. In general, E_c of single crystals is lower than those of ceramics with the same composition due to unclamped domain wall motion and relatively easy P_s^i reversal [18]. Therefore, by extension to polycrystalline materials, grain size has a considerable effect on the electromechanical properties of ferroelectrics [174–177]. An optimal grain size is obtained when a maximized density of domains (and domain walls) leads to a proper balance between non-180° switchable domains and minimized back switching [176–179]. Excessive grain size leads to deterioration of dielectric and electromechanical properties due to disproportionate back switching [177]. On the other hand, too small grain size leads to suppression of ferroelectricity due to diminished non-cubic distortions [180–182]. Moreover, domains also become unfavorable at small grain sizes since P_s is compensated by interface charges at grain boundaries and/or polarization gradients [182]. This leads initially to a single domain state, followed by complete suppression of the ferroelectric state as grain size is further reduced [183]. For $PbTiO_3$ the critical grain size to induce a paraelectric state is between 4 nm and 20 nm [184, 185], while for BT it is between 10 nm and 100 nm [180–182]. BT has maximized properties at grain sizes between 1 μm and 2 μm [178, 179]. Optimization of grain size leads in general to higher ε_r', lower T_C, decreased E_c, and increased d_{33}, and d_{33}^* [174, 175, 178]. Typically grain size can be altered by modifications to the raw starting powders, as well as by modifications of calcination and sintering processes [186].

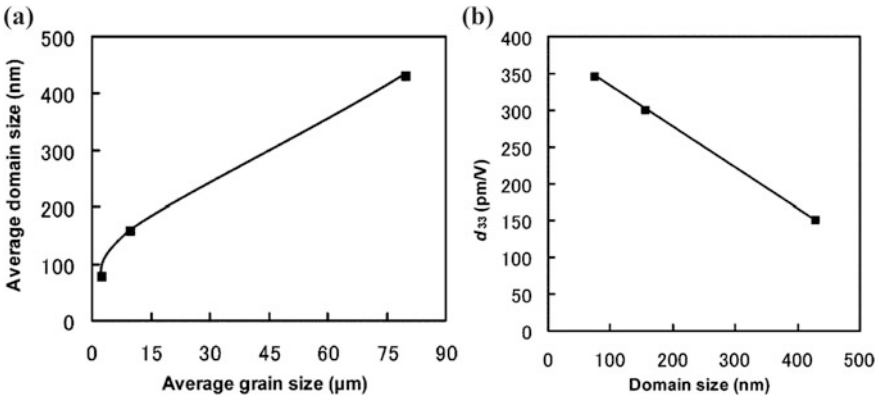

Fig. 2.18 **a** Relation between grain size and domain size. **b** Relation between d_{33} and domain size for BT. Adapted from Takahashi [197] with permission of John Wiley & Sons

It was suggested that domain size is proportional to the square root of the grain size [187, 188]. However, the relation remains valid only for grain sizes in the micrometer range [18] and in compositions far from phase instabilities [158]. Several works on BT determine that a fine domain structure can greatly contribute to its piezoelectric activity [189–197]. Moreover, charged domains walls were also mentioned as further enhancing the piezoelectricity of materials with fine domains [198]. Figure 2.18 introduces the relation between (a) grain size and domain size and (b) domain size and d_{33}.

In general, enhanced electromechanical properties observed in materials with reduced domain size are associated with an increased domain wall density and their enhanced mobility [124, 199, 200]. Domain engineering refers to a technique employed to induce a stable and optimized domain size in a material so that maximized functional properties can be achieved [124, 125, 199]. Although domain size and grain size are related in polycrystalline materials (Fig. 2.18a), domain engineering is also effective in single crystals [201, 202]. Although coarse domain configurations generally feature diminished functional properties, they give rise to increased electric field and temperature stability [202].

2.3.2.2 Texturing

Apart from grain and domain engineering, the electromechanical properties can be further enhanced by texturing. Wada and Pulpan [203, 204] determined that the [110]-oriented BT with an average domain size of 800 nm and grain size of 75 μm features a $d_{33} = 788$ pC/N. Moreover, texturing was also shown to be a potential strategy to enhance the temperature stability of electromechanical properties [106]. It also has the advantage that it does not lower the operational temperature range

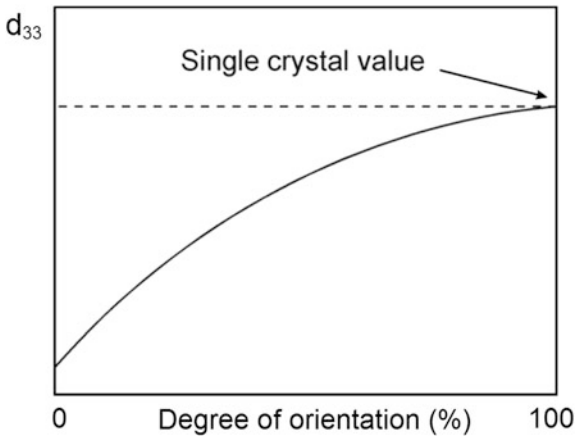

Fig. 2.19 Piezoelectric response given by d_{33} as a function of degree of orientation. Adapted from Leontsev and Eitel [124]

[20]. Texturing enhances the electromechanical response of ferroelectrics because the inherent anisotropy of ferroelectrics does not allow a fully oriented domain state along the applied electric field [20, 205]. Therefore, the limit of properties enhancement is given by the single crystal material variant, as displayed schematically in Fig. 2.19.

The most commonly used texturing methods in ferroelectrics are templated grain growth and reactive templated grain growth [205]. Nevertheless, magnetic field texturing has also yielded promising results for some systems [206]. Orientation degrees between 60 % and 90 % have been achieved in lead-free ferroelectrics leading to enhancement of the electromechanical properties between 20 % and 200 % [20].

2.3.2.3 Design of Heterogeneous Materials

Although chemical and structural modifications are the most common approaches for the production of new ceramics, further alternatives are available to improve the functional properties of ferroelectrics. Design of composite and core-shell materials affords extra variables to tailor this functionality, such as through connectivity and interface engineering. A proper design affects both intrinsic and extrinsic contributions to the piezoelectric activity. Figure 2.20 displays schematic views of the heterogeneous microstructures that have so far been attempted to tailor large signal electromechanical properties in lead-free piezoelectrics. Figure 2.20a introduces a 0–3 composite (Newnham's notation [207]) and (b) an approximate $(1_5; 1_\infty)_i$ core-shell microstructure. The generalized nomenclature for core-shell geometries is introduced in Appendix I.

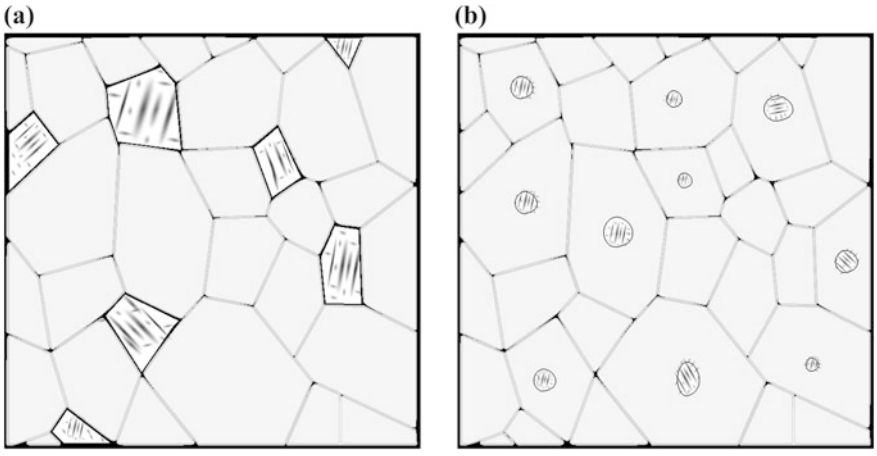

Fig. 2.20 Schematic representation of heterogeneous materials **a** 0–3 composites and **b** an approximate $(1_5; 1_\infty)_i$ core-shell microstructure. Macroscopically polar seeds such as a ferroelectric or non-ergodic relaxor state are displayed with presence of domain contrast, while gray regions designate a macroscopically non-polar matrix such as a paraelectric or ergodic relaxor state

The composite approach is suited to engineer lead-free incipient piezoelectrics. For this purpose, 0–3 BNT-based composites were designed with a macroscopically polar seed such as a ferroelectric or non-ergodic relaxor state in conjunction with a macroscopically non-polar matrix such as a paraelectric or ergodic relaxor state [208–215]. This approach allowed for an enhanced strain output with reduced hysteresis, which gave between 10 % and 30 % higher electromechanical response than solid solution materials at 4 kV/mm [208, 211]. The feasibility of tailoring the temperature and frequency stability with the composite approach was also demonstrated at the expense of reduced strain output [212]. The large signal strain and polarization, as well as the small signal dielectric properties, were calculated successfully in several works based on a model that regarded the microstructural constituents as two capacitors in series [209, 211, 216]. Since the charge of two capacitors in series is equal, the applied macroscopic electric field is distributed differently between constituents to assure a constant polarization. Generally, the macroscopically non-polar matrix depicts lower $\frac{\partial P}{\partial E}$ indicating that the electric field on the matrix will be higher. This promotes the electric field induced phase transition of incipient piezoelectrics and thus gives rise to their high electromechanical response at lower applied electric fields. Although these models considered only polarization coupling between the constituents, it was recently proposed that strain coupling should also play an important role [217, 218]. Apart from the effect of changing the electric field distribution, it was suggested that the electric field induced phase transformation should be aided due to heterogeneous nucleation at the interfaces between constituents [208, 209, 214]. Theoretically it was demonstrated that nucleation and domain switching occur through a self-organized behavior that is electrostatically controlled during initial stages and elastostatically controlled at later stages [217].

The composite approach increases the complexity of the synthesis process. Difference in thermal expansion coefficients and/or the lattice mismatch between constituents should be considered as limiting factors since they can lead to defects and/or low density. Moreover, the interface between constituents can act as nucleation site of parasitic phases that can be detrimental to attaining the desired functional properties [219, 220]. This reduces the attractiveness of this approach for industrial applications and hence highlights the potential of core-shell materials since they can be processed in situ during a conventional solid state route. Core-shell materials have experienced an increased interest due to technologically relevant dielectric [221–227], piezoelectric [228], and multiferroic [219, 229] properties. Within nanotechnology developments, there has been a continuous increase in organic and inorganic core-shell nanoparticle discoveries with exceptional properties [230]. A promising lead-free core-shell piezoceramic was developed by Choi et al. [228]. in the $CaZrO_3$-modified (K,Na)(Nb,Ta)O_3. This system depicted an exceptional $d^*_{33} > 1000$ pm/V at 3 kV/mm but only within a limited temperature range. The high strain of the system was attributed to the presence of a reversible poled state in the Ta^{5+}-rich non-polar shell indicating an analogous strain mechanism with composites. Although BNT-based core-shell microstructures have been

previously reported, the functional properties associated with this microstructure were not addressed [231, 232]. Moreover, an inspection of literature reveals that certain BNT-based piezoceramics may exhibit a core-shell microstructure although its effect on the functional properties was not discussed [233].

Bibliography

1. P. Zubko, G. Catalan, A.K. Tagantsev, Annu. Rev. Mater. Res. **43**, 387 (2013)
2. D.E. Aspnes, Am. J. Phys. **50**, 704 (1982)
3. F. Cardarelli, *Materials Handbook: A Concise Desktop Reference. Chapter 8: Insulators and Dielectrics* (Springer, 2008)
4. C. Kittel, *Introduction to Solid State Physics. Chapter 13: Dielectrics and Ferroelectrics* (Wiley, 1996)
5. K.C. Kao, *Dielectric Phenomena in Solids* (Elsevier Academic Press, 2004)
6. M. Lallart, *Ferroelectrics: Characterization and Modeling* (InTech, 2011)
7. H.F. Kay, Rep. Prog. Phys. **18**, 230 (1955)
8. M.E. Lines, A.M. Glass, *Principles and Applications of Ferroelectrics and Related Material* (Oxford University Press, 1977)
9. R. Waser, U. Böttger, S. Tiedke, *Polar Oxides* (Wiley-VCH, 2005)
10. B.A. Strukov, A.P. Levanyuk, *Ferroelectric Phenomena in Crystals: Physical Foundations* (Springer, 1998)
11. J.F. Nye, *Physical Properties of Crystals* (Oxford University Press, 1967)
12. R.E. Newnham, *Properties of Materials Anisotropy: Anisotropy, Symmetry, Structure* (Oxford University Press, 2005)
13. B. Jaffe, W.R. Cook, H. Jaffe, *Piezoelectric Ceramics* (Academic Press London, 1971)
14. F. Jona, G. Shirane, *Ferroelectric Crystals* (Dover Publications, 1993)
15. K. Rabe, C.H. Ahn, J.M. Triscone, *Physics of Ferroelectrics: A Modern Perspective* (Springer, 2007)
16. A. Safari, E.K. Akdogan, *Piezoelectric and Acoustic Materials for Transducer Applications* (Springer, 2008)
17. D. Damjanovic, Rep. Prog. Phys. **61**, 1267 (1998)
18. L. Jin, F. Li, S. Zhang, J. Am. Ceram. Soc. **97**, 1 (2014)
19. G.H. Haertling, J. Am. Ceram. Soc. **82**, 797 (1999)
20. J. Rödel, W. Jo, K.T.P. Seifert, E.M. Anton, T. Granzow, D. Damjanovic, J. Am. Ceram. Soc. **92**, 1153 (2009)
21. J. Rödel, A.B.N. Kounga, M. Weissenberger-Eibl, D. Koch, A. Bierwisch, W. Rossner, M. J. Hoffmann, R. Danzer, G. Schneider, J. Eur. Ceram. Soc. **29**, 1549 (2009)
22. D.A. Porter, *Phase Transformations in Metals and Alloys* (Chapman & Hall, 1996)
23. E.K.H. Salje, ChemPhysChem **11**, 940 (2010)
24. D. Damjanovic, J. Am. Ceram. Soc. **88**, 2663 (2005)
25. K. Uchino, *Ferroelectric Devices* in *Materials Science and Technology: A Comprehensive Treatment*, vol 11 (1994)
26. A.A. Bokov, Z.G. Ye, J. Mater. Sci. **41**, 31 (2006)
27. Z.G. Ye, Key Eng. Mater. **155–156**, 81 (1998)
28. L.E. Cross, Ferroelectrics **76**, 241 (1987)
29. G.A. Samara, E.L. Venturini, Phase Transitions **79**, 21 (2006)
30. P.N. Timonin, Ferroelectrics **400**, 427 (2010)
31. W. Kleemann, J. Mater. Sci. **41**, 129 (2006)
32. V.V. Shvartsman, D.C. Lupascu, J. Am. Ceram. Soc. **95**, 1 (2012)
33. V. Gopalan, D.B. Litvin, Nat. Mater. **10**, 376 (2011)

34. M.Y. Gureev, A.K. Tagantsev, N. Setter, Phys. Rev. B **83**, 184104 (2011)
35. W. Cao, L.E. Cross, Phys. Rev. B **44**, 5 (1991)
36. H.L. Hu, L.Q. Chen, J. Am. Ceram. Soc. **81**, 492 (1998)
37. G. Arlt, D. Hennings, G. de With, J. Appl. Phys. **58**, 1619 (1985)
38. T. Egami, Ferroelectrics **267**, 101 (2002)
39. J. Valasek, Phys. Rev. **17**, 475 (1921)
40. W.L. Cherry, R. Adler, Phys. Rev. **72**, 981 (1947)
41. S. Roberts, Phys. Rev. **71**, 890 (1947)
42. B.T. Matthias, Phys. Rev. **75**, 1771 (1949)
43. G.H. Kwei, A.C. Lawson, S.J.L. Billinge, S.W. Cheong, J. Phys. Chem. **97**, 2368 (1993)
44. W. Zhong, D. Vanderbilt, Phys. Rev. Lett. **74**, 2587 (1995)
45. Q.M. Zhang, W.Y. Pan, S.J. Jang, L.E. Cross, J. Appl. Phys. **64**, 6445 (1988)
46. D.A. Hall, Ferroelectrics **223**, 319 (1999)
47. M. Vopsaroiu, J. Blackburn, M.G. Cain, P.M. Weaver, Phys. Rev. B **82**, 024109 (2010)
48. S.E. Park, T.R. Shrout, J. Appl. Phys. **82**, 1804 (1997)
49. G.A. Smolenskii, V.A. Isupov, Sov. Phys. Solid State **24**, 1375 (1954)
50. G.A. Smolenskii, V.A. Isupov, A.I. Agranovskaya, N.N. Krainik, Sov. Phys. Solid State **2**, 2651 (1961)
51. G.A. Smolenskii, V.A. Isupov, A.I. Agranovskaya, S.N. Popov, Sov. Phys. Solid State **2**, 2584 (1961)
52. G. Burns, F.H. Dacol, Solid State Commun. **48**, 853 (1983)
53. G. Burns, F.H. Dacol, Ferroelectrics **104**, 25 (1990)
54. P. Bonneau, P. Garnier, G. Calvarin, E. Husson, J.R. Gavarri, A.W. Hewat, A. Morell, J. Solid State Chem. **91**, 350 (1991)
55. C. Malibert, B. Dkhil, J.M. Kiat, D. Durand, J.F. Berar, A. Spasojevic-de Bire, J. Phys. Condens. Matter **9**, 7485 (1997)
56. N. Takesue, Y. Fujii, M. Ichihara, H. Chen, Phys. Lett. A **257**, 195 (1999)
57. P. Ganesh, E. Cockayne, M. Ahart, R.E. Cohen, B. Burton, R.J. Hemley, Y. Ren, W. Yang, Z.G. Ye, Phys. Rev. B **81**, 144102 (2010)
58. D. La-Orauttapong, J. Toulouse, J. Robertson, Z.G. Ye, Phys. Rev. B **64**, 212101 (2001)
59. D. Viehland, S.J. Jang, L.E. Cross, M. Wuttig, J. Appl. Phys. **68** (1990)
60. D. Viehland, M. Wuttig, L.E. Cross, Ferroelectrics **120**, 71 (1991)
61. A.J. Bell, J. Phys.: Condens. Matter **5**, 8773 (1993)
62. W. Kleemann, Int. J. Mod. Phys. B **7**, 2469 (1993)
63. W. Kleemann, Phase Transitions **65**, 141 (1998)
64. W. Kleemann, A. Klossner, Ferroelectrics **150**, 35 (1993)
65. V. Westphal, W. Kleemann, M. Glinchuk, Phys. Rev. Lett. **68**, 847 (1992)
66. R. Blinc, J. Dolinsek, B. Gregorovic, B. Zalar, C. Filipic, Z. Kutnjak, A. Levstik, R. Pirc, J. Phys. Chem. Solids **61**, 177 (2000)
67. R. Blinc, B. Gregorovic, B. Zalar, R. Pirc, S.G. Lushnikov, Phys. Rev. B **61**, 253 (2000)
68. R. Pirc, R. Blinc, Phys. Rev. B **60**, 13470 (1999)
69. R. Pirc, R. Blinc, V. Bobnar, Ferroelectrics **259**, 169 (2001)
70. R. Pirc, R. Blinc, V. Bobnar, Phys. Rev. B **63**, 054203 (2001)
71. A.E. Glazounov, A.K. Tagantsev, Ferroelectrics **221**, 57 (1999)
72. A.K. Tagantsev, A.E. Glazounov, Phys. Rev. B **57**, 18 (1998)
73. T. Komatsuzaki, A. Baba, S. Kawai, M. Toda, J.E. Straub, R.S. Berry, *Advancing Theory for Kinetics and Dynamics of Complex, Many-Dimensional Systems: Clusters and Proteins* (Wiley, 2011), p. 171
74. C.R. Oliveira, T. Werlang, Rev. Bras. Ensino Fisica **29**, 189 (2007)
75. D.L. Stein, AIP Conf. Proc. **1389**, 965 (2011)
76. H. Vogel, Phys. Z. **22**, 645 (1921)
77. G. Fulcher, J. Am. Ceram. Soc. **8**, 339 (1925)
78. R. Pirc, R. Blinc, Phys. Rev. B **76**, 020101 (2007)
79. A. Levstik, Z. Kutnjak, C. Filipič, R. Pirc, Phys. Rev. B **57**, 11204 (1998)

80. V. Bobnar, Z. Kutnjak, R. Pirc, A. Levstik, Phys. Rev. B **60**, 6420 (1999)
81. N. Novak, R. Pirc, M. Wencka, Z. Kutnjak, Phys. Rev. Lett. **109**, 037601 (2012)
82. W. Jo, J.E. Daniels, D. Damjanovic, W. Kleemann, J. Rödel, Appl. Phys. Lett. **102**, 192903 (2013)
83. E.M. Anton, W. Jo, D. Damjanovic, J. Rödel, J. Appl. Phys. **110**, 094108 (2011)
84. K. Uchino, Ferroelectrics **151**, 321 (1994)
85. L.E. Cross, S.J. Jang, R.E. Newnham, S. Nomura, K. Uchino, Ferroelectrics **23**, 187 (2011)
86. M.B. Rauls, W. Dong, J.E. Huber, C.S. Lynch, Acta Mater. **59**, 2713 (2011)
87. Z.G. Ye, A.A. Bokov, Ferroelectrics **302**, 227 (2004)
88. H. Khemakhem, A. Simon, R.V.D. Mühll, J. Ravez, J. Phys. Condens. Matter **12**, 5951 (2000)
89. J. Ravez, R. Von der Mühll, A. Simon, P. Sciau, J. Mater. Chem. **9**, 2829 (1999)
90. J. Ravez, C. Broustera, A. Simon, J. Mater. Chem. **9**, 1609 (1999)
91. A. Aydi, H. Khemakhem, C. Boudaya, A. Simon, R. Von der Mühll, Solid State Sci. **7**, 249 (2005)
92. C. Ma, X. Tan, J. Am. Ceram. Soc. **94**, 4040 (2011)
93. H.S. Han, W. Jo, J. Rödel, I.K. Hong, W.P. Tai, J.S. Lee, J. Phys. Condens. Matter **24**, 365901 (2012)
94. V.D.N. Tran, H.S. Han, C.H. Yoon, J.S. Lee, W. Jo, J. Rödel, Mater. Lett. **65**, 2607 (2011)
95. R. Dittmer, W. Jo, J.E. Daniels, S. Schaab, J. Rödel, J. Am. Ceram. Soc. **94**, 4283 (2011)
96. Y. Hiruma, H. Nagata, T. Takenaka, J. Appl. Phys. **104**, 124106 (2008)
97. Y. Hiruma, H. Nagata, T. Takenaka, Appl. Phys. Lett. **95**, 052903 (2009)
98. Y. Hiruma, H. Nagata, T. Takenaka, Jpn. J. Appl. Phys. **48**, 09KC08 (2009)
99. A. Hussain, C.W. Ahn, J.S. Lee, A. Ullah, I.W. Kim, Sens. Actuators, A **158**, 84 (2010)
100. A. Hussain, C.W. Ahn, A. Ullah, J.S. Lee, I.W. Kim, Jpn. J. Appl. Phys. **49**, 041504 (2010)
101. A. Hussain, J.U. Rahman, A. Zaman, R.A. Malik, J.S. Kim, T.K. Song, W.J. Kim, M.H. Kim, Mater. Chem. Phys. **143**, 1282 (2014)
102. W. Jo, E. Erdem, R.A. Eichel, J. Glaum, T. Granzow, D. Damjanovic, J. Rödel, J. Appl. Phys. **108**, 014110 (2010)
103. A. Maqbool, A. Hussain, J.U. Rahman, T. Kwon Song, W.J. Kim, J. Lee, M.H. Kim, Ceram. Int. **40**, 11905 (2014)
104. V.Q. Nguyen, H.S. Han, K.J. Kim, D.D. Dang, K.K. Ahn, J.S. Lee, J. Alloy. Compd. **511**, 237 (2012)
105. K.N. Pham, A. Hussain, C.W. Ahn, W. Kim III, S.J. Jeong, J.S. Lee, Mater. Lett. **64**, 2219 (2010)
106. Y. Saito, H. Takao, T. Tani, T. Nonoyama, K. Takatori, T. Homma, T. Nagaya, M. Nakamura, Nature **432**, 84 (2004)
107. K.T.P. Seifert, W. Jo, J. Rödel, J. Am. Ceram. Soc. **93**, 1392 (2010)
108. A. Ullah, C.W. Ahn, A. Hussain, I.W. Kim, H.I. Hwang, N.K. Cho, Solid State Commun. **150**, 1145 (2010)
109. K. Wang, A. Hussain, W. Jo, J. Rödel, J. Am. Ceram. Soc. **95**, 2241 (2012)
110. K. Wang, F.Z. Yao, W. Jo, D. Gobeljic, V.V. Shvartsman, D.C. Lupascu, J.F. Li, J. Rödel, Adv. Funct. Mater. **23**, 4079 (2013)
111. S.T. Zhang, A.B. Kounga, E. Aulbach, H. Ehrenberg, J. Rödel, Appl. Phys. Lett. **91**, 112906 (2007)
112. A. Ullah, C.W. Ahn, A. Hussain, S.Y. Lee, H.J. Lee, I.W. Kim, Curr. Appl. Phys. **10**, 1174 (2010)
113. S.T. Zhang, A.B. Kounga, E. Aulbach, T. Granzow, W. Jo, H.J. Kleebe, J. Rödel, J. Appl. Phys. **103**, 034107 (2008)
114. W. Jo, T. Granzow, E. Aulbach, J. Rödel, D. Damjanovic, J. Appl. Phys. **105**, 094102 (2009)
115. M. Hinterstein, M. Knapp, M. Hölzel, W. Jo, A. Cervellino, H. Ehrenberg, H. Fuess, J. Appl. Crystallogr. **43**, 1314 (2010)
116. J.E. Daniels, W. Jo, J. Rödel, J.L. Jones, Appl. Phys. Lett. **95**, 032904 (2009)

117. A.J. Royles, A.J. Bell, A.P. Jephcoat, A.K. Kleppe, S.J. Milne, T.P. Comyn, Appl. Phys. Lett. **97**, 132909 (2010)
118. A.J. Royles, A.J. Bell, J.E. Daniels, S.J. Milne, T.P. Comyn, Appl. Phys. Lett. **98**, 182904 (2011)
119. H. Simons, J.E. Daniels, W. Jo, R. Dittmer, A. Studer, M. Avdeev, J. Rödel, M. Hoffman, Appl. Phys. Lett. **98**, 082901 (2011)
120. H. Simons, J.E. Daniels, J. Glaum, A.J. Studer, J.L. Jones, M. Hoffman, Appl. Phys. Lett. **102**, 062902 (2013)
121. H. Simons, J.E. Daniels, A.J. Studer, J.L. Jones, M. Hoffman, J. Electroceram. **32**, 283 (2014)
122. J. Kling, X. Tan, W. Jo, H.J. Kleebe, H. Fuess, J. Rödel, J. Am. Ceram. Soc. **93**, 2452 (2010)
123. E. Sapper, N. Novak, W. Jo, T. Granzow, J. Rödel, J. Appl. Phys. **115**, 194104 (2014)
124. S.O. Leontsev, R.E. Eitel, Sci. Technol. Adv. Mater. **11**, 044302 (2010)
125. F. Li, L. Wang, L. Jin, D. Lin, J. Li, Z. Li, Z. Xu, S. Zhang, IEEE Trans. Ultrason. Ferroelectr. Freq. Control **62**, 18 (2015)
126. V.M. Goldschmidt, Naturwissenschaften **14**, 477 (1926)
127. W. Jo, J.E. Daniels, J.L. Jones, X. Tan, P.A. Thomas, D. Damjanovic, J. Rödel, J. Appl. Phys. **109**, 014110 (2011)
128. J.F. Li, K. Wang, F.Y. Zhu, L.Q. Cheng, F.Z. Yao, J. Am. Ceram. Soc. **96**, 3677 (2013)
129. J. Rödel, K.G. Webber, R. Dittmer, W. Jo, M. Kimura, D. Damjanovic, J. Eur. Ceram. Soc. **35**, 1659 (2015)
130. K. Wang, J.F. Li, J. Adv. Ceram. **1**, 24 (2012)
131. A.A. Heitmann, G.A. Rossetti Jr, J. Am. Ceram. Soc. **97**, 1661 (2014)
132. D. Damjanovic, IEEE Trans. Ultrason. Ferroelectr. Freq. Control **56**, 1574 (2009)
133. A.G. Khachaturyan, Phil. Mag. **90**, 37 (2010)
134. G.A. Rossetti Jr, A.G. Khachaturyan, G. Akcay, Y. Ni, J. Appl. Phys. **103**, 114113 (2008)
135. Y. Ishibashi, Ferroelectrics **264**, 197 (2001)
136. A.A. Heitmann, G.A. Rossetti Jr, Phil. Mag. **90**, 71 (2010)
137. D. Damjanovic, M. Budimir, M. Davis, N. Setter, J. Mate. Sci. **41**, 65 (2006)
138. Y. Ishibashi, M. Iwata, Jpn. J. Appl. Phys. **38**, 1454 (1999)
139. M. Iwata, Y. Ishibashi, Jpn. J. Appl. Phys. **38**, 5670 (1999)
140. M. Iwata, H. Orihara, Y. Ishibashi, Jpn. J. Appl. Phys. **40**, 703 (2001)
141. M. Davis, M. Budimir, D. Damjanovic, N. Setter, J. Appl. Phys. **101**, 054112 (2007)
142. K. Carl, K.H. Härdtl, Phys. Status Solidi A **8**, 87 (1971)
143. W. Cochran, Adv. Phys. **9**, 387 (1960)
144. D. Damjanovic, Appl. Phys. Lett. **97**, 062906 (2010)
145. B. Noheda, D.E. Cox, G. Shirane, J.A. Gonzalo, L.E. Cross, S.E. Park, Appl. Phys. Lett. **74**, 2059 (1999)
146. R. Guo, L.E. Cross, S.E. Park, B. Noheda, D.E. Cox, G. Shirane, Phys. Rev. Lett. **84**, 5423 (2000)
147. B. Noheda, Curr. Opin. Solid State Mater. Sci. **6**, 27 (2002)
148. B. Noheda, D.E. Cox, Phase Transitions **79**, 5 (2006)
149. W.F. Rao, Y.U. Wang, Appl. Phys. Lett. **90**, 182906 (2007)
150. D. Pandey, A.K. Singh, S. Baik, Acta Crystallogr. Sect. A **64**, 192 (2008)
151. M. Davis, J. Electroceram. **19**, 25 (2007)
152. Crystallographic tables A1: Symmetry relations between space groups. Accesible online in http://www.cryst.ehu.es/cryst/cellsub.html, (05/07/2015)
153. Y.M. Jin, Y.U. Wang, A.G. Khachaturyan, J.F. Li, D. Viehland, J. Appl. Phys. **94**, 3629 (2003)
154. D. Viehland, J. Appl. Phys. **88**, 4794 (2000)
155. Y.U. Wang, Phys. Rev. B **76**, 024108 (2007)
156. J. Frantti, Y. Fujioka, A. Puretzky, Y. Xie, Z.G. Ye, A.M. Glazer, J. Appl. Phys. **113**, 174104 (2013)

157. R. Kirchhofer, D.R. Diercks, B.P. Gorman, J.F. Ihlefeld, P.G. Kotula, C.T. Shelton, G.L. Brennecka, J. Am. Ceram. Soc. **97**, 2677 (2014)
158. G.A. Rossetti Jr, A.G. Khachaturyan, Appl. Phys. Lett. **91**, 072909 (2007)
159. W.F. Rao, Y.U. Wang, Appl. Phys. Lett. **91**, 052901 (2007)
160. R. Theissmann, L.A. Schmitt, J. Kling, R. Schierholz, K.A. Schönau, H. Fuess, M. Knapp, H. Kungl, M.J. Hoffmann, J. Appl. Phys. **102**, 024111 (2007)
161. L. Jin, Z. He, D. Damjanovic, Appl. Phys. Lett. **95**, 012905 (2009)
162. M. Budimir, D. Damjanovic, N. Setter, Phys. Rev. B **73**, 174106 (2006)
163. Z. Kutnjak, J. Petzelt, R. Blinc, Nature **441**, 956 (2006)
164. Z. Kutnjak, R. Blinc, Phys. Rev. B **76**, 104102 (2007)
165. M. Porta, T. Lookman, A. Saxena, J. Phys. Condens. Matter **22**, 345902 (2010)
166. N. Novak, R. Pirc, Z. Kutnjak, Phys. Rev. B **87**, 104102 (2013)
167. Z.K. Liu, X. Li, Q.M. Zhang, Appl. Phys. Lett. **101**, 082904 (2012)
168. M.J. Haun, E. Furman, S.J. Jang, L.E. Cross, Ferroelectrics **99**, 13 (1989)
169. W. Liu, X. Ren, Phys. Rev. Lett. **103**, 257602 (2009)
170. C. Zhou, W. Liu, D. Xue, X. Ren, H. Bao, J. Gao, L. Zhang, Appl. Phys. Lett. **100**, 222910 (2012)
171. L.F. Zhu, B.P. Zhang, X.K. Zhao, L. Zhao, F.Z. Yao, X. Han, P.F. Zhou, J.F. Li, Appl. Phys. Lett. **103**, 072905 (2013)
172. L. Jin, V. Porokhonskyy, D. Damjanovic, Appl. Phys. Lett. **96**, 242902 (2010)
173. D.M. Smyth, *The Defect Chemistry of Metal Oxides* (Oxford University Press, 2000)
174. C.A. Randall, N. Kim, J.P. Kucera, W. Cao, T.R. Shrout, J. Am. Ceram. Soc. **81**, 677 (1998)
175. J. Hao, W. Bai, W. Li, J. Zhai, J. Am. Ceram. Soc. **95**, 1998 (2012)
176. P. Zheng, J.L. Zhang, Y.Q. Tan, C.L. Wang, Acta Mater. **60**, 5022 (2012)
177. Y. Tan, J. Zhang, C. Wang, G. Viola, H. Yan, Phys. Status Solidi A **212**, 433 (2015)
178. Y. Tan, J. Zhang, Y. Wu, C. Wang, V. Koval, B. Shi, H. Ye, R. McKinnon, G. Viola, H. Yan, Scientific reports **5**, Article number: 9953 (2015)
179. D. Ghosh, A. Sakata, J. Carter, P.A. Thomas, H. Han, J.C. Nino, J.L. Jones, Adv. Funct. Mater. **24**, 885 (2014)
180. K. Uchino, E. Sadanaga, T. Hirose, J. Am. Ceram. Soc. **72**, 1555 (1989)
181. S. Tsunekawa, S. Ito, T. Mori, K. Ishikawa, Z.Q. Li, Y. Kawazoe, Phys. Rev. B **62**, 3065 (2000)
182. Z. Zhao, V. Buscaglia, M. Viviani, M.T. Buscaglia, L. Mitoseriu, A. Testino, M. Nygren, M. Johnsson, P. Nanni, Phys. Rev. B **70**, 024107 (2004)
183. G. Arlt, J. Mater. Sci. **25**, 2655 (1990)
184. K. Ishikawa, K. Yoshikawa, N. Okada, Phys. Rev. B **37**, 5852 (1988)
185. A. Roelofs, T. Schneller, K. Szot, R. Waser, Appl. Phys. Lett. **81**, 5231 (2002)
186. W.D. Kingery, H.K. Bowen, D.R. Uhlmann, *Introduction to Ceramics* (Wiley, 1976)
187. W. Cao, C.A. Randall, J. Phys. Chem. Solids **57**, 1499 (1996)
188. G. Arlt, Ferroelectrics **104**, 217 (1990)
189. H. Takahashi, Y. Numamoto, J. Tani, K. Matsuta, J. Qiu, S. Tsurekawa, Jpn. J. Appl. Phys. **45**, L30 (2006)
190. H. Takahashi, Y. Numamoto, J. Tani, S. Tsurekawa, Jpn. J. Appl. Phys. **45**, 7405 (2006)
191. T. Karaki, K. Yan, T. Miyamoto, M. Adachi, Jpn. J. Appl. Phys. **46**, L97 (2007)
192. H. Takahashi, Y. Numamoto, J. Tani, S. Tsurekawa, Jpn. J. Appl. Phys. **46**, 7044 (2007)
193. T. Karaki, K. Yan, M. Adachi, Appl. Phys. Express **1**, 111402 (2008)
194. S. Shao, J. Zhang, Z. Zhang, P. Zheng, M. Zhao, J. Li, C. Wang, J. Phys. D Appl. Phys. **42**, 189801 (2009)
195. Z.Y. Shen, J.F. Li, J. Ceram. Soc. Jpn. **118**, 940 (2010)
196. N. Ma, B.P. Zhang, W.G. Yang, D. Guo, J. Eur. Ceram. Soc. **32**, 1059 (2012)
197. H. Takahashi, Electron. Commun. Jpn **95**, 20 (2012)
198. T. Sluka, A.K. Tagantsev, D. Damjanovic, M. Gureev, N. Setter, Nature Commun. **3**, 748 (2012)

199. T. Higuchi, K. Suzumori, S. Tadokoro, *Next-Generation Actuators Leading Breakthroughs* (Springer, London, 2010)
200. S. Wada, K. Yako, H. Kakemoto, T. Tsurumi, T. Kiguchi, J. Appl. Phys. **98**, 014109 (2005)
201. S. Wada, T. Tsurumi, Br. Ceram. Trans. **103**, 1 (2004)
202. D. Lin, S. Zhang, Z. Li, F. Li, Z. Xu, S. Wada, J. Luo, T.R. Shrout, J. Appl. Phys. **110**, 084110 (2011)
203. S. Wada, P. Pulpan, Key Eng. Mater. **421–422**, 13 (2009)
204. S. Wada, K. Takeda, T. Muraishi, H. Kakemoto, T. Tsurumi, T. Kimura, Ferroelectrics **373**, 11 (2008)
205. G.L. Messing, S. Trolier-McKinstry, E.M. Sabolsky, C. Duran, S. Kwon, B. Brahmaroutu, P. Park, H. Yilmaz, P.W. Rehrig, K.B. Eitel, E. Suvaci, M. Seabaugh, K.S. Oh, Crit. Rev. Solid State Mater. Sci. **29**, 45 (2004)
206. J. Zhao, F. Wang, W. Li, H. Li, D. Zhou, S. Gong, Y. Hu, Q. Fu, J. Appl. Phys. **108**, 073535 (2010)
207. R.E. Newnham, D.P. Skinner, L.E. Cross, Mater. Res. Bull. **13**, 525 (1978)
208. D.S. Lee, D.H. Lim, M.S. Kim, K.H. Kim, S.J. Jeong, Appl. Phys. Lett. **99**, 062906 (2011)
209. D.S. Lee, S.J. Jeong, M.S. Kim, J.H. Koh, J. Appl. Phys. **112**, 124109 (2012)
210. D.S. Lee, S.J. Jeong, M.S. Kim, K.H. Kim, Jpn. J. Appl. Phys. **52**, 021801 (2013)
211. C. Groh, D.J. Franzbach, W. Jo, K.G. Webber, J. Kling, L.A. Schmitt, H.J. Kleebe, S.J. Jeong, J.S. Lee, J. Rödel, Adv. Funct. Mater. **24**, 356 (2014)
212. C. Groh, W. Jo, J. Rödel, J. Appl. Phys. **115**, 234107 (2014)
213. C. Groh, W. Jo, J. Rödel, J. Am. Ceram. Soc. **97**, 1465 (2014)
214. S.J. Jeong, D.S. Lee, M.S. Kim, S.M. Jang, I.S. Kim, S. Mohsin, J.S. Song, J. Electroceram. **33**, 230 (2014)
215. N.H. Khansur, C. Groh, W. Jo, C. Reinhard, J.A. Kimpton, K.G. Webber, J.E. Daniels, J. Appl. Phys. **115**, 124108 (2014)
216. T. Shrout, W.A. Schulze, J.V. Biggers, Ferroelectrics **29**, 129 (2011)
217. J.E. Zhou, T.L. Cheng, Y.U. Wang, J. Appl. Phys. **111**, 024105 (2012)
218. H. Zhang, C. Groh, Q. Zhang, W. Jo, K.G. Webber, J. Rödel, Adv. Electron. Mater. **6** doi:10.1002/aelm.201500018 (2015)
219. G. Schileo, Prog. Solid State Chem. **41**, 87 (2013)
220. L. Mitoseriu, V. Buscaglia, Phase Transitions **79**, 1095 (2006)
221. Z. Zhigang, Z. Weilong, W. Yugong, Z. Ruitao, Ferroelectrics **101**, 55 (1990)
222. C.A. Randall, S.F. Wang, D. Laubscher, J.P. Dougherty, W. Huebner, J. Mater. Res. **8**, 871 (1993)
223. Y. Park, Y. Kim, J. Mater. Res. **10**, 2770 (1995)
224. Y. Park, H.G. Kim, J. Am. Ceram. Soc. **80**, 106 (1997)
225. Y. Sakabe, N. Wada, T. Hiramatsu, T. Tonogaki, Jpn. J. Appl. Phys. **41**, 6922 (2002)
226. H. Tian, J. Qi, Y. Wang, H.L.W. Chan, C.L. Choy, Prog. Solid State Chem. **33**, 207 (2005)
227. G. Yang, Z. Yue, Z. Gui, L. Li, J. Appl. Phys. **104**, 074115 (2008)
228. S.Y. Choi, S.J. Jeong, D.S. Lee, M.S. Kim, J.S. Lee, J.H. Cho, B.I. Kim, Y. Ikuhara, Chem. Mater. **24**, 3363 (2012)
229. R.P. Mahajan, K.K. Patankar, M.B. Kothale, S.C. Chaudhari, V.L. Mathe, S.A. Patil, Pramana **58**, 1115 (2002)
230. R.G. Chaudhuri, S. Paria, Chem. Rev. **112**, 2373 (2012)
231. S.Y. Cheng, J. Shieh, N.J. Ho, H.Y. Lu, Phil. Mag. **91**, 4013 (2011)
232. S.Y. Cheng, J. Shieh, H.Y. Lu, C.Y. Shen, Y.C. Tang, N.J. Ho, J. Eur. Ceram. Soc. **33**, 2141 (2013)
233. W. Krauss, D. Schütz, F.A. Mautner, A. Feteira, K. Reichmann, J. Eur. Ceram. Soc. **30**, 1827 (2010)

http://www.springer.com/978-3-319-27755-4

Strain Mechanisms in Lead-Free Ferroelectrics for Actuators

Acosta, M.

2016, XVIII, 181 p. 105 illus., 86 illus. in color.,
Hardcover
ISBN: 978-3-319-27755-4